UNIVERSITY OF TURIN

DOCTORAL SCHOOL IN LIFE AND HEALTH SCIENCES

PhD in Medical Pathophysiology - Cycle XXXIII

The role of TNFα-induced protein 2 (TNFAIP2) in diabetic nephropathy

Candidate:

Stefania BELLINI

Tutor:

Prof. Gabriella GRUDEN

INDEX

List of Abbreviations (in order of appearance)

DN: diabetic nephropathy

TNTs: tunneling nanotubes

TNFAIP2: TNFα-induced protein 2; TNFα: tumor necrosis factor

HG: high glucose concentration; NG: normal glucose concentration

GA: glycated albumin

MS: mechanical stretch

KO: knock-out

T1DM: type 1 diabetes; T2DM: type 2 diabetes

ESRD: end stage renal disease

CV: cardiovascular

ACR: albumin-to-creatinine ratio

eGFR: estimated glomerular filtration rate

CDK-EPI: Chronic Kidney Disease Epidemiology Collaboration

KDIGO: Kidney Disease - Improving Global Outcomes

CKD: chronic kidney disease

GBM: glomerular basement membrane

DCCT: Diabetes Control and Complications Trial

AGEs: advanced glycation-end products

TGF-β1: transforming growth factor β1

CTGF: connective tissue growth factor

VEGF: vascular endothelial growth factor

MCP-1: monocyte chemoattractant protein 1

CCR2: C-C chemokine receptor type 2

mtDNA: mitochondrial DNA

RAS: renin-angiotensin system

TNFR1: TNFα receptor 1; TNFR2: TNFα receptor 2

NF-κB: nuclear factor kappa-light-chain-enhancer of activated B cells

ACE-I: angiotensin-converting-enzyme inhibitors

ARB: angiotensin II receptor blockers

SGLT2i: sodium-glucose transport protein 2 inhibitors

RAGE: advanced glycation end-products receptors

MSCs: mesenchymal stem cells

HIV: human immunodeficiency virus

GFP: green fluorescent protein

HUVEC: human umbilical vein endothelial cells

LPS: lipopolysaccharide

FSGS: focal segmental glomerulosclerosis

AD: Adriamycin

PECs: parietal epithelial cells

TFAM: mitochondrial transcriptional factor A

COX1: cytochrome c oxidase subunit I

ND4L: NADH-ubiquinone oxidoreductase chain 4L

PRKDC: DNA-dependent protein kinase catalytic subunit

TBE: Tris-borate-EDTA buffer

STZ: streptozotocin

NeoR: neomycin resistance

HSV: herpes simplex virus

PCR: polymerase chain reaction

AER: albumin excretion rate

SBP: systolic blood pressure

HPLC: high-performance liquid chromatography

ADMCC: Animal Models of Diabetic Complications Consortium

HBSS: Hank's balanced salt solution

BM: bone marrow

TUNEL: terminal deoxynucleotidyl transferase dUTP nick end labeling

FCS: fetal calf serum

shRNA: short hairpin RNA

WGA: wheat germ agglutinin

RFP: red fluorescent protein

PAS: periodic acid-Schiff

YAG: yttrium aluminium garnet

CCD: charge-coupled device

LY6C2: lymphocyte antigen 6 complex, locus C2

HPRT: hypoxanthine-guanine phosphoribosyltransferase 1

WT-1: Wilms' tumor protein

GAPDH: glyceraldehyde 3-phosphate dehydrogenase

BSA: bovine serum albumin

PBS: phosphate buffered saline

HRP: horseradish peroxidase

FITC: fluorescein isothiocyanate

RPE: R-phycoerythrin

RIPA: radioimmunoprecipitation assay buffer

SDS: sodium dodecyl sulfate

TBS: tris-buffered saline

SEM: standard error of the mean

ANOVA: analysis of variance

DM: diabetic

ND: non diabetic

WT: wild type

KW/BW: kidney weight/body weight ratio

BP: blood pressure

CrCl: creatinine clearance

BG: blood glucose

Abstract

Background. Diabetic nephropathy (DN) is characterized by both albuminuria and relentless decline in renal function. Podocyte damage/loss and organelle dysfunction play a key role in the pathogenesis of the complication. Identification of novel mechanisms of podocyte repair/organelle replacement would be important to effectively target podocyte injury in DN. Tunneling nanotubes (TNTs) are membrane channels interconnecting cells and allowing transfer of subcellular components, including organelles, from donor to recipient injured cells. The cytosolic protein TNFα-induced protein 2 (TNFAIP2) plays a key role in TNT formation in various cell types, including podocytes. The general purpose of the present study was thus to explore the potential relevance of the TNFAIP2-TNT system in the context of DN.

Methods. First, we studied glomerular TNFAIP2 both expression and distribution in renal biopsies from patients with DN and in the renal cortex of streptozotocin-induced diabetic mice. Second, we assessed the effect of global TNFAIP2 deletion on functional, structural, and molecular abnormalities of early experimental DN. Finally, we investigated *in vitro* in cultured podocytes whether diabetes-related insults [high glucose (HG), glycated albumin (GA), mechanical stretch (MS)] affect TNFAIP2 expression, TNT formation, and TNT-mediated mitochondrial exchange.

Results. TNFAIP2 was overexpressed by podocytes in patients with DN and in experimental diabetes. TNFAIP2 deletion exacerbated both functional and structural abnormalities of DN. Specifically, diabetic TNFAIP2-KO mice showed worsening of albuminuria, renal function, podocyte damage, and glomerular both inflammation and fibrosis. Transplantation of $TNFAIP2^{+/+}$ bone marrow cells did not rescue the renal phenotype of diabetic $TNFAIP2^{-/-}$ mice.

In cultured podocytes, HG induced TNFAIP2 expression, and both HG and GA enhanced TNT formation in an Akt/PI3K/TNFAIP2-dependent manner. GA-induced TNTs were functionally active as they allowed mitochondrial transfer. *Conclusions.* Both diabetes-induced TNFAIP2 overexpression in podocytes and worsening of DN in TNFAIP2 KO mice suggest a protective effect of TNFAIP2 in the context of diabetes. Our *in vitro* data provide a possible explanation for the beneficial effects of TNFAIP2, as TNT formation in response to diabetes-related insults was TNFAIP2-dependent and allowed mitochondrial transfer.

1. Introduction

1.1 Diabetic nephropathy and glomerular damage

The number of people living with diabetes has dramatically increased in the last decades. According with the International Diabetes Federation, currently almost 500 million adults are living with diabetes globally and these figures are predicted to reach 700 million by 2045 [1].

Diabetic nephropathy is a microvascular complication of diabetes affecting approximately 30-40% of type 1 (T1DM) and type 2 (T2DM) diabetic patients. DN is a major cause of end-stage renal disease (ESRD), requiring renal replacement therapy. Moreover, DN is an important risk factor of cardiovascular (CV) both morbidity and mortality and most people with DN die because of CV complications prior to ESRD development [2-4]. Both epidemiological and intervention studies have demonstrated a central role of both hyperglycemia and hypertension in both the onset and the progression of the complication [5-10].

Clinical features. DN is characterized both albuminuria and progressive renal function decline, leading to ESRD. Severely increased and persistent albuminuria (macroalbuminuria) is a hallmark of overt DN, while a moderate increase in albuminuria (microalbuminuria) is considered an early phase of the complication and predicts the future development of established DN [11]. Table 1 shows the cut-off values for the definition of micro- and macroalbuminuria. DM patients undergo annual screening for early detection of albuminuria (starting at diagnosis in T2DM patients and after 5 years from diagnosis in T1DM patients). Screening is usually performed by measuring the albumin-to-creatinine ratio (ACR) in a morning urine sample. Because of the variability in albuminuria at least 2 out of 3 positive tests carried out over a period of 3-6 months are required

to make the diagnosis of micro-/macro-albuminuria. DN screening also includes the annual assessment of renal function by measurement of serum creatinine. Glomerular filtration rate (eGFR) is estimated using the Chronic Kidney Disease Epidemiology Collaboration (CDK-EPI, https://www.kidney.org/professionals/kdoqi/gfr) equation and stratified in 5 stages according to the National Kidney Foundation. The classification by the Kidney Disease: Improving Global Outcomes (KDIGO) estimates the patient global risk (both renal and CV) based on both albuminuria and CKD stages [12].

Table 1. Definition of albuminuria categories

Measure	**Urinary albumin category**		
	Normal	Moderate increase (micro-albuminuria)	Severe increase (macro-albuminuria)
Albumin Excretion Rate 24 hour-collection	<30 mg/24h	30-299 mg/24h	>300 mg/24h
Albumin Excretion Rate Overnight collection	<20 µg/min	20-199 µg/min	>200 µg/min
Albumin-to-creatinine Ratio Spot sample	<30 mg/g	30-299 mg/g	>300 mg/g

Histopathological features. Podocyte abnormalities, thickening of the glomerular basement membrane (GBM), excessive extracellular matrix accumulation in the mesangium, and tubulointerstitial fibrosis are characteristic features of DN [13]. Podocytes are highly specialized epithelial cells that wrap around the outer surface of the glomerular capillaries being a key component of the glomerular filtration barrier. The *slit diaphragm* - a junction between adjacent podocyte foot processes - is the ultimate restriction site of the glomerular filtration system that prevents blood proteins leaking into urine. Downregulation of *slit diaphragm* proteins, such as

nephrin and podocin, is found in human DN and pathogenically linked to albuminuria. Other podocyte abnormalities include cytoskeleton alterations, foot process effacement, reduced adhesion to the GBM, and podocyte apoptosis [14-16]. The main histopathological features of DN are shown in Figure 1.

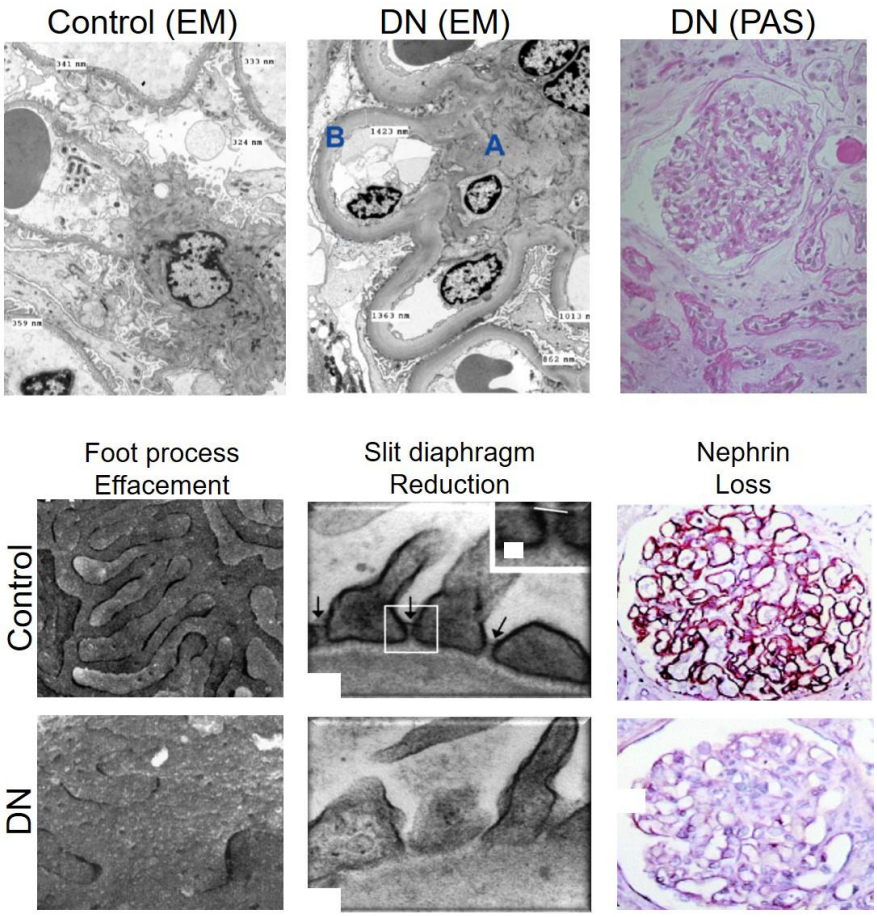

Figure 1. Histopathological features of diabetic nephropathy (DN). *Top left*: Electron microscope (EM) images of glomerular structural changes in DN compared to control. *A* indicates marked expansion of the mesangium; *B* indicates marked diffuse thickening of the glomerular basement membrane (to three times the normal thickness in this case). *Top right*: Periodic acid-Schiff (PAS) staining of renal biopsy from microalbuminuric type 2 diabetic patient showing mild mesangial expansion, interstitial fibrosis and tubular atrophy. *Bottom*: EM and immunohistochemical staining images showing podocyte alterations in DN as compared to control subjects: foot process effacement, slit diaphragm reduction and nephrin loss.

Pathogenesis.

Hyperglycemia. Both epidemiological and intervention studies have proven that hyperglycemia plays a key role in the pathogenesis of DN. Among them of particular importance were the Diabetes Control and Complications Trial (DCCT) and the United Kingdom Prospective Diabetes Study in type 1 and type 2 diabetic patients, respectively [5-7]. *In vivo* and *in vitro* studies have clarified that exposure of mesangial cells to high glucose/hyperglycemia induces cell hypertrophy and increased production/reduced degradation of extracellular matrix components [17]. In addition, a high glucose milieu also affects podocytes by inducing nephrin loss, podocyte apoptosis, and foot processes effacement [18, 19]. The deleterious effects of hyperglycemia are due to both enhanced glucose entry into glomerular cells via the Glut-1 transporter as well as increased formation of advanced glycosylation-end products (AGEs). The increased flux of glucose into cells alters the cellular phenotype through activation of intracellular signaling molecules/pathways (protein kinase C, aldose reductase pathway, and hexosamine pathway). Moreover, a number of cytokines, such as transforming growth factor β1 (TGF-β1), connective tissue growth factor (CTGF), vascular endothelial growth factor (VEGF), monocyte chemoattractant protein 1 (MCP-1), are induced by high glucose concentrations and contribute to the glomerular injury by inducing sclerosis, inflammation and enhanced permeability [20, 21].

Hyperglycemia and Organelle Dysfunction. There is increasing evidence that organelle dysfunction plays an important role in the pathogenesis of DN. Lysosomal alterations have been reported and autophagy, a lysosomal pathway involved in the removal of damaged organelles, is altered in diabetic mice and in podocytes exposed to high glucose concentrations [22]. Furthermore, impaired autophagy has been shown to sensitize podocytes toward glomerular diseases and to contribute to podocyte injury in the diabetic kidney [23]. Mitochondrial

abnormalities, such as swollen/fragmented mitochondria, altered mitochondrial membrane potential, and impaired permeability transition, have also been demonstrated in renal cells exposed to a diabetic milieu and in the kidneys from diabetic animals [24-27]. Moreover, the "unifying hypothesis" has postulated that excessive generation of mitochondrial superoxide by hyperglycemia is the primary initiating event that activates all other pathways of glomerular damage in diabetes [28]. Hyperglycemia-induced mitochondrial oxidative stress can also cause mutations of mitochondrial DNA (mtDNA). Although mtDNA has a high degree of redundancy, these mutations may accumulate in terminally differentiated cells, such as podocytes, and lead to permanent alterations in mitochondrial bioenergetics [29].

Hypertension. Hypertension contributes to the progression of DN and intervention studies have convincingly shown that anti-hypertensive treatment can slow the progression of the complication [8-10]. Besides systemic hypertension, the vasodilation of the afferent arteriole in diabetes induces an increase in glomerular capillary pressure that plays a key role in the glomerular damage. Indeed, blockers of the renin-angiotensin system (RAS) are particularly effective in delaying the progression of DN because they can diminish intraglomerular pressure levels [30]. *In vitro* studies have clarified the mechanisms whereby glomerular hypertension results in glomerular injury. Glomeruli have a high degree of compliance; therefore, glomerular hypertension causes pulsatile glomerular expansion with stretching of glomerular cells. By exposing glomerular cells to mechanical stretch, mimicking glomerular capillary hypertension, *in vitro* studies have shown that mechanical stretch can enhance both TGF-β1 and extracellular molecule production in mesangial cells [31, 32] and nephrin loss/apoptosis in podocytes [33, 34]. Therefore, glomerular hypertension mimics and magnifies the deleterious effect of hyperglycemia on glomerular cells.

Inflammation. Inflammatory processes have been implicated in the pathogenesis and progression of the renal injury in diabetes [35]. Glomerular infiltration of monocytes/macrophages has been proven in both human and experimental diabetes. The chemokine MCP-1 is overexpressed by glomerular cells exposed to a high glucose milieu and mediates glomerular monocyte accrual, leading to chronic low-grade inflammation [36, 37]. Inflammatory cytokines and in particular MCP-1 and Tumor necrosis factor α (TNFα) magnify the deleterious effects of high glucose on both mesangial cells and podocytes and contribute to the development of albuminuria and to renal function decline. In particular, binding of TNFα to the TNFR1 and TNFR2 receptors, leading to NF-κB activation, enhances production of extracellular matrix components in mesangial cells and induces cytoskeleton alteration, nephrin redistribution and loss, and apoptosis in podocytes [38, 39]. Consistent with the hypothesis that micro inflammation is important in the pathogenesis of DN, studies in animal models of diabetes have proven that blockade of inflammation ameliorates experimental DN [40, 41].

Treatment. Blood glucose control and RAS blockade with either ACE inhibitors (ACE-I) or angiotensin II receptor antagonists (ARB) are effective in reducing DN onset/progression. Additionally, there is evidence that sodium-glucose cotransporter 2 inhibitors (SGLT2i) have an anti-proteinuric and renoprotective effect even in patients already treated with RAS inhibitors, though the underlying mechanism/s have not been fully clarified [42]. Despite improvement in DN treatment, a proportion of patients still progress to more advanced stages of the disease. There is, thus, the need to find novel targets for intervention.

1.2 Tunneling nanotubes (TNTs) and TNFα-induced protein 2 (TNFAIP2)

Structural and functional features of TNTs. Tunneling nanotubes (TNTs) are a novel mechanism of cell-to-cell communication. TNTs are membranous straight bridges, interconnecting cells. They have a F-actin and/or microtube backbone, are 50-500 nm wide, and span distances up to several cell diameters. TNTs lack adhesion to the substrate, and this distinguishes TNTs from filopodia [43] (Figure 2). The formation of either TNTs or filopodia appears to be mutually exclusive: when the molecular machinery required for filopodia formation (CDC42-IRSp53-VASP) is activated, TNTs formation is inhibited; on the contrary, when the actin regulatory protein Esp8 promotes TNT formation, filopodia assembling is suppressed [44].

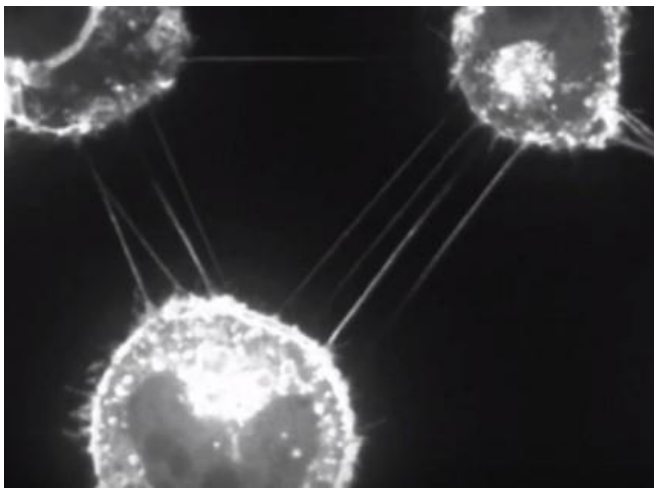

Figure 2. Representative image of three cells interconnected by tunnelling nanotubes (TNTs). The image shows bridging-like straight membranous channels connecting cells over distances spanning up to several cell diameters, being 50-500 nm wide, and lacking adhesion to the substrate.

Role of TNTs in pathophysiological contexts. TNTs have been demonstrated in several cell types *in vitro*, such as monocytes/macrophages, endothelial, cancer, immune, and stem cells [43]. Cells form TNTs *de novo* in response to stress – including serum starvation, hypoxia, and oxidative stress - suggesting that TNTs may serve as a survival mechanism. However, TNTs are also involved in physiological processes, such as osteoclast differentiation [45], electrical coupling and calcium signaling [46]. The mechanisms for TNT direction guidance have not been clarified yet; however, in astrocytes both the calcium binding protein S100A4 and the RAGE receptor have been implicated in TNT guidance [47].

TNTs mediate the exchange of various factors, such as ions, nucleic acids, and proteins. TNT-mediated calcium signaling contributes to communication between neurons [46] and dendritic cells use TNT connections for intercellular exchange of antigens [48]. At variance with other intercellular communication system TNTs also allow exchange of organelles, including lysosomes and mitochondria [43, 49, 50]. TNT-mediated mitochondria transfer was observed in several cell types, including endothelial cells, bone marrow-derived stromal cells, astrocytes [51-53], and mesenchymal stem cells (MSCs). Of interest, mitochondrial transfer from MSCs to recipient cells can even rescue mitochondrial respiration in recipient mitochondrial-depleted cells [50, 54, 55]. Likely, the ability to replace dysfunctional organelles *via* TNTs is an important survival mechanism and is particularly relevant in terminally differentiated cells.

However, TNTs may also contribute to cell damage. In fact, TNTs can favor the spreading of viruses, such as HIV, herpes and influenza viruses, prions and bacteria [56-58]. Moreover, an increasing number of studies have shed light on the deleterious role of TNTs in cancer. Indeed, malignant cells take advantage of TNTs to drive tumor both formation and progression, and to acquire chemoresistance [59]. Finally, in neurodegenerative diseases, TNTs allow spreading of

deleterious components, such as prion-like proteins, polyglutamine aggregates, α-synuclein, facilitating propagation of protein misfolding [49, 60, 61].

In vivo relevance of TNTs. TNTs are very sensitive to light, mechanical stresses, and chemical fixation procedures, making it difficult to identify and visualize TNTs in living tissues. Despite these technical issues, recent studies succeeded in the identification of TNT-like structures either *in vivo* or *in situ*. By labeling cells with GFP and using lattice-light sheet microscopy, Parker et al visualized TNTs interconnecting breast cancer metastatic cells in murine brain slides [62]. Another study demonstrated that glioblastoma cell lines implanted in brain surgical lesions developed functionally active TNTs [63]. Recently, Alarcon-Martinez et al. provided *in vivo* evidence of the existence of TNTs interconnecting pericytes in the mouse retina. By using two-photon laser-scanning microscopy, mito-Dendra2 mice, and calcium indicators, the Authors also showed mitochondria traveling along TNT-like structures and demonstrated that TNT-mediated calcium waves mediate cell-to-cell communication in the living retinas [64].

Central role of TNFAIP2 in TNT formation. TNFα-induced protein 2 (TNFAIP2), also known as B94 or m-Sec is a cytoplasmic protein of 73 kDa. It was first identified as a primary response gene induced by TNFα in human umbilical vein epithelial cells (HUVEC), but interleukin 1-β and LPS can also induce TNFAIP2 mRNA expression in this cell type. During embryonic mouse development, TNFAIP2 has been identified in several tissues, including the myocardium, the liver, and the kidney [65]. Post-natal expression of TNFAIP2 was predominantly found in lymphopoietic tissues, mononuclear progenitor cells, and mature peripheral monocytes. In addition, a testis-specific truncated form of TNFAIP2 transcript was identified in the acrosomal compartment of mature sperm [66].

In 2009 Ohno et al. demonstrated a central role for TNFAIP2 in TNT formation. Indeed, they showed that TNFAIP2 is required for TNT formation in Raw264.7 macrophages and that TNFAIP2 induces TNTs by interacting with RalA and the exocyst complex, a downstream effector of Ral [67]. In particular, TNFAIP2 interacts with the plasma membrane via the N-terminal region and recruits active RalA to extend the plasma membrane protrusion via the positive charged C-terminus [68]. The signaling molecules leading to TNFAIP2-depedent TNT formation has not been fully elucidated; however, p53 and the Akt/PI3K/m-TOR signaling pathway have been involved [69]. The importance of TNFAIP2 in TNT development has been demonstrated several other cell types, including immune, HeLa, and HEK293T cells [70].

1.3 Role of the TNFAIP2-TNT system in the kidney

We recently demonstrated that the TNFAIP2-TNT system plays an important role in focal segmental glomerulosclerosis (FSGS) [71]. In FSGS, podocyte injury/loss is an early event, leading to the development of proteinuria. This is followed by glomerular scarring that is both focal and segmental in distribution. We found that TNFAIP2 is overexpressed by podocytes in kidney biopsies from patients with FSGS as well as in experimental FSGS (Adriamycin (AD)-induced nephropathy).

To clarify if TNFAIP2 overexpression in FSGS was either a compensatory/protective response to injury or a mechanism of glomerular damage, we generate a TNFAIP2 knockout (KO) mouse. TNFAIP2-KO mice on a Balb/c genetic background were viable, fertile and grew normally. However, TNFAIP2 deletion led to the spontaneous development of FSGS with aging. Indeed, glomerulosclerosis affected some, but not all glomeruli, fulfilling the definition of focal glomerular

lesions and led to a relentless renal function decline. Podocyte injury, resulting in podocytopenia and albuminuria, occurred prior to the development of visible renal lesions by light microscopy. Activated $CD44^{+}$-PECs that have been proposed as a diagnostic tool to identify patients with FSGS were found in both the Bowman's capsule and the glomerular tuft.

Both TNFAIP2-KO mice and primary podocytes from $TNFAIP2^{-/-}$ animals showed mitochondrial abnormalities, such as reduced mtDNA copy number, downregulation of mitochondrial transcriptions factors/genes (TFAM, COX1, ND4L), and altered mitochondria bioenergetics. This suggests that lack of mitochondrial exchange via TNTs secondary to TNFAIP2 deficiency may functionally link TNFAIP2 deletion to renal injury. Consistent with this hypothesis, we found that stressed podocytes (exposed to either serum deprivation or AD) form TNTs in TNFAIP2-dependent manner. Moreover, TNT-mediated mitochondrial transfer can occur between podocytes and is enhanced towards podocytes exposed to insults inducing mitochondrial dysfunctions. Finally, re-expression of TNFAIP2 not only re-established podocyte ability to form TNTs and exchange mitochondria, but also rescued podocytes from mitochondrial dysfunction, nephrin downregulation and apoptosis. This work showed the importance of the TNFAIP2-TNT in FSGS, but it is unknown whether this system is also of relevance in other kidney diseases, including DN (Figure 3). As reported above, Balb/c TNFAIP2-KO mice spontaneously develop FSGS; however, the Balb/c strain is prone to develop FSGS [72], likely because of a mutation in the PRKDC gene that is important in mitochondrial genome repair [73]. Therefore, we cannot exclude the possibility that deletion of TNFAIP2 in other murine strains and in particular in C57BL6, which are resistant to FSGS development may result in a more benign renal phenotype.

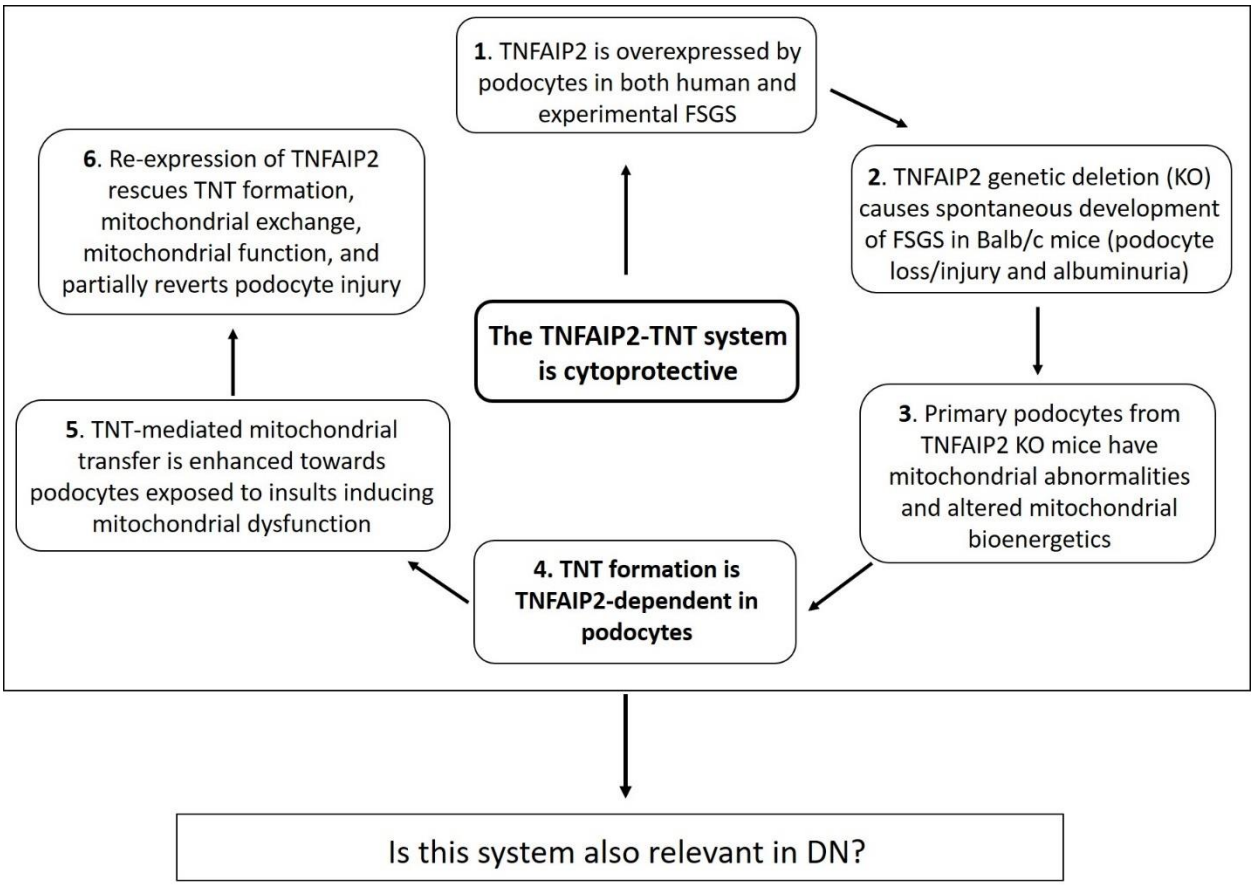

Figure 3. Role of the TNFAIP2-TNT system in the kidney. The flow-chart reports the main experimental evidences indicating the protective role of the TNFAIP2-TNT system in focal segmental glomerulosclerosis (FSGS). These evidences suggested a possible role for the TNFAIP2-TNT system also in diabetic nephropathy (DN).

2. Aim of the study

Diabetic nephropathy (DN) is characterized by both albuminuria and relentless decline in renal function. Podocyte damage/loss plays a key role in the pathogenesis of the complication and identification of novel mechanisms of podocyte repair is important to target podocyte injury in DN.

Tunneling nanotubes (TNTs) are membrane tunnels interconnecting cells and allowing transfer of organelles from donors to injured recipient cells. The cytosolic protein TNFα-induced protein 2 (TNFAIP2) is crucial for TNT formation in various cell types, including podocytes. We have recently reported that TNFAIP2 is overexpressed by podocytes in FSGS and that blockade of the TNFAIP2-TNT system by knocking down TNFAIP2 induces the spontaneous development of FSGS in Balb/c mice. The general purpose of the present project is to explore the potential relevance of the TNFAIP2-TNT system in the context of DN. Specifically, our aims were:

1. to assess glomerular TNFAIP2 expression in human kidney biopsies from patients with DN and in a murine model of DN;
2. to establish if global TNFAIP2 deletion affects both structural and functional alterations of DN in the streptozotocin (STZ)-induced murine model of diabetes and to clarify the underlying mechanisms;
3. to clarify *in vitro* whether podocyte exposure to diabetes-related insults affects TNT formation and this occurs in a TNFAIP2-dependent manner.
4. to explore whether diabetes-induced TNTs are functionally active and mediate intercellular organelle exchange.

3. Research Design and Methods

3.1 Human study

Archival Serra's fluid-fixed paraffin-embedded kidney biopsies were provided by the Department of Internal Medicine of Genoa University. Kidney sections from type 2 diabetic patients with either incipient (*n*=3, 30-300 mg/24h) or overt nephropathy (*n*=12, persistent proteinuria >0.5 g/24h) were studied. Sections from diabetic patients showed glomerular alterations and the histological features of DN; kidney biopsies presenting a different pattern of damage such as vascular and interstitial damage were excluded from the study. Normal renal tissue was obtained from subjects (*n*=8), who underwent surgery for localized grade I hypernephroma, and used as control tissue. Samples were selected based on the absence of proteinuria and glomerular abnormalities as assessed by both light and immunofluorescence microscopy. The study was approved by the Ethical Committee of Genoa University, all procedures were in accordance with the Helsinki Declaration, and an informed consent was obtained from all subjects.

Hypertension was defined as a blood pressure ≥140/90 mmHg on at least three different occasions. Twenty-four–hour urinary protein content was measured using the pyrogallol-red method in three separate urine collections. Serum creatinine was assessed using the Jaffé method. All clinical procedures were conducted in accordance with the Helsinki Declaration. Creatinine clearance was estimated using the Cockcroft-Gault formula, and glycated haemoglobin measured by ion-exchange chromatography technique.

3.2 Animal study

Male C57BL6 were purchased from Charles River Laboratories Italia. Animal studies were approved by the Ethical Committee of the Turin University and both housing and care of laboratory animals were in accordance with the Italian law. Animals were maintained on a normal diet under standard animal housing conditions.

Generation of TNFAIP2 knockout (KO) mice on a C57Bl6 genetic background.

Mice with global TNFAIP2 deletion (TNFAIP2-KO) were kindly provided by Prof. Ohno H (Riken, Japan). To generate TNFAIP2 KO mice, the target vector containing a 4-kb genomic sequence (promoter), neomycin resistance (NeoR) cassette floxed at both ends, a 3.5-kb genomic fragment (intron5-exon10) and the HSV-tk gene, was constructed with pBluescript II SK (+). The linearized targeting vector was inserted into B6;129 hybrid embryonic stem cells. The correctly targeted cells were screened by long range-PCR. Chimeric mice were bred with C57BL6 mice to obtain germline-transmitted animals. The obtained heterozygous were then crossed with transgenic mice expressing a CAG promoter-controlled Cre recombinase to remove the NeoR gene, and backcrossed to C57BL/6 mice for 8 generations before inter-crossing to obtain homozygous. TNFAIP2 deletion was confirmed by Southern blot analysis.

Genotyping. Genomic DNA was extracted and purified from mouse-tail tissue using the PureLink Genomic DNA kit (Thermo Fisher Scientific). Genotyping was performed by traditional semi-quantitative PCR, using the following primers:

TNFAIP2 WT 5’TCTCCTTCTTCTTCGCAGACTC3’

TNFAIP2 KO 5’TGAAGCTACAAACTGCTCTGCC3’

TNFAIP2-common 5’GGTCCTGGTGTTTTTACTGGAC3’

After an initial denaturation at 94°C for 2 minutes, the DNA was amplified for 35 cycles with the following PCR protocol: denaturation at 98°C for 10 seconds, annealing at 60°C for 30 seconds, and elongation at 68°C for 1 minute. PCR products were resolved in a 2% agarose/TBE gel containing ethidium bromide and digital images captured using the Gel Doc XR system (Bio-Rad, Milan, Italy).

Streptozotocin-induced diabetes. Diabetes was induced in eight-week-old mice by intraperitoneal injection of streptozotocin (STZ) diluted in citrate buffer, pH 4.5 (55 mg/kg body weight/day), delivered in five consecutive daily doses. Mice that were sham injected with sodium citrate buffer were used as controls. Diabetes onset was confirmed by blood glucose levels >250 mg/dL four weeks after the first STZ dose. Before euthanasia, blood samples were collected via saphenous vein puncture on alert 4-h-fasted animals. Glucose levels were measured using a glucometer (Accu-chek; Roche, Milan, Italy) and glycated hemoglobin by quantitative immunoturbidimetric latex determination (Sentinel Diagnostic, Milan, Italy). Systolic blood pressure (SBP) was assessed by tail-cuff plethysmography. Urinary albumin was measured by enzyme-linked immunosorbent assay (Bethyl Laboratories, Milan, Italy) in 18-h urine collections as either albumin excretion rate (AER, µg/18h) or albumin-to-creatinine ratio (ACR µg/mg). For 18-h urine collection, animals were individually housed into metabolic cages where water and food were accessible *ad libitum*. Creatinine clearance was calculated from serum and urine creatinine concentrations, as determined by HPLC according to the Animal Models of Diabetic Complications Consortium (ADMCC) guidelines [74]. Twelve weeks after diabetes onset, mice were killed by decapitation. The kidneys were rapidly dissected, weighed, and processed for subsequent analyses. Half a kidney was formalin-fixed and paraffin-embedded for light

microscopy analyses and the other half was OCT-included and snap-frozen in liquid nitrogen. The second kidney was stored at -80°C for RNA and protein analyses. In all experimental groups, some kidneys were used for glomeruli isolation.

Glomerular Isolation. Deeply anesthetized animals were perfused at a constant flow rate (8ml/min) with an HBSS solution containing $8x10^7$ surface-inactivated magnetic beads (Dynabeads, Invitrogen, Milan, Italy). The kidneys were removed, finely minced, digested for 30 minutes at 37°C in a solution containing collagenase (1 mg/ml) and DNAse (100 U/ml), and then passed through a 100 μm mesh. Cell suspensions were collected by centrifugation and glomeruli gathered using a magnetic particle concentrator and then repeatedly washed to remove tubules. Purity was assessed by light microscopy.

Bone marrow (BM) transplantation study. Eight-week-old male TNFAIP2-KO and WT mice were used as bone marrow (BM) donors. BM cells were flushed from tibial and femoral cavities under sterile conditions, filtered through 70 μm nylon meshes (BD Biosciences, Milan, Italy), and then transplanted without further purification or *in vitro* expansion. Before transplantation, recipient male mice, aged 8 weeks, underwent whole body-irradiation (8 Gy). After 24 hours, post-irradiated mice were injected with $2.0x10^6$ BM cells via the tail vein. TNFAIP2-KO mice received a BM transplant from either WT (KO-c^{WT}; n=5) or KO (KO-c^{KO}; n=5) animals and WT recipients from WT-c^{WT}; n=5) animals. DNA was isolated from blood cells (DNeasy Blood and Tissue Kit, Qiagen, Milan, Italy) and chimerism confirmed by PCR.

Apoptosis. Apoptotic cells were detected on renal cortical sections by transferase-mediated dUTP nick end-labeling (TUNEL) assay (ApopTag In Situ Apoptosis Detection Kit, Millipore, Billerica, MA). Results were expressed as the number of positive cells per glomerulus (at least 20 random glomeruli).

3.3 *In vitro* study

Cell culture. Conditionally immortalized human podocytes were kindly provided by Prof. Saleem. Cells, were cultured and expanded at 33°C, 5% CO_2, in RPMI medium, containing 10% fetal calf serum (FCS), 100U/mL of penicillin/streptomycin, 2mM L-glutamine, insulin, transferrin and sodium selenite. Subsequent experiments were performed using podocytes differentiated at 37°C.

Diabetes-related insults. Conditionally immortalized human podocytes were exposed to high glucose concentrations (HG, [glucose] = 30mM), glycated-albumin (GA 1.2µg/ml) for 48h, or mechanical stretch for 24h. Cells exposed to normal glucose concentrations (NG= 10 mM made iso-osmolar with mannitol), vehicle, or cultured in a hemodynamic stable environment were used as controls. In a subset of experiments, the Akt inhibitor VIII (1 µM) and the PI3K inhibitor (LY294002, 50 µM) were also added.

sh-RNA. Conditionally immortalized human podocytes ($3x10^5$) were transfected using Lipofectamine 3000 Transfection Reagent (Thermo Fisher Scientific) with a plasmid construct encoding TNFAIP2-specific sh-RNA (shRNA: 5'-GATCCGACTGCTGGAGGCCACATTCCTGT-3', scramble negative control: 5'-GCACTACCAGAGCTAACTCAGATAGTACT-3') cloned in a pGFP-V-RS vector (ExactHuSH, OriGene Technologies Inc). Knockdown efficiency was assessed by western blotting.

TNTs. To visualize plasma membrane and TNTs, podocytes were labeled with 5 µg/ml of WGA conjugated with Alexa Fluor®-488 (Thermo Fisher Scientific, Milan, Italy) in HBSS for 10 minutes at 37°C. The number of cells connected by straight WGA-labeled structures that did not adhere to the substrate, as assessed by Z-stack, and with diameter smaller than 1 µm was counted

in blind and results expressed as percentage of total counted cells (at least 150 cells). To visualize TNT actin-based backbone, podocytes were labeled with Cell-Light Actin RFP (Molecular Probes, Thermo Fisher Scientific, Milan Italy), and then co-cultured with podocytes exposed to normal glucose concentrations (NG = 10 mM).

Mitochondrial transfer. Cell-Tracker Blue CMAC Dye (Molecular Probes, Thermo Fisher Scientific, Milan Italy), a cytoplasmic dye suitable for long-term cell tracing, was used at 5μM concentration to label recipient cells. Donor cells were labeled with Mitotracker Red dye (Thermo Fisher Scientific) at the concentration of 25 nM.

Recipient cells were pre-treated with GA (1.2 μg/ml) and then co-cultured with donor cells at a ratio of 1:1 in IbiTreated μ-dish for 24 hours. Fluorescence was used to visually assess mitochondrial transfer. To control for TNT-independent transfer, the two cell populations were separately seeded into a 2 Well Ibidi Culture-Insert, sharing the same culture medium. After cell attachment, the insert was removed and the two populations co-cultured for 24 hours under gentle shaking.

3.4 Microscopy

Light Microscopy. Paraffin-embedded renal sections were stained using Periodic acid–Schiff (PAS). Mesangial area was analyzed (percentage of glomerular area) from digital pictures of 15–20 glomeruli per kidney per animal using the Axiovision 4.7 software (Milan, Italy).

Electron Microscopy. Renal cortex pieces (1 mm^3) were fixed in 2% glutaraldehyde, 4% paraformaldehyde in phosphate buffer 0.12 mol/l for 4 h at room temperature, postfixed in 1% osmium tetroxide for 2 h, dehydrated in graded ethanol, and embedded in Epon 812. Ultrathin

sections (70 nm thickness) were obtained with a Leica EM UC6 ultramicrotome, counterstained with uranyl acetate and lead citrate, and examined with an Energy Filter Transmission Electron Microscope (EFTEM, ZEISS LIBRA® 120) equipped with an yttrium aluminium garnet (YAG) scintillator slow scan charge-coupled device (CCD) camera (Sharp eye, TRS, Moorenweis, Germany).

Fluorescent and DIC microscopy. A Zeiss APOTOME 2 system equipped with an incubator for live cell imaging/time-lapse microscopy and Nomarski optics for differential interference contrast (DIC) microscopy was used in TNT studies. DIC microscopy was used to avoid TNT phototoxic damage. Sequences of optical planes (Z-stack) were acquired for reconstruction in the x-z plane.

3.5 mRNA analysis

Total RNA was extracted and purified from renal cortex, isolated glomeruli, and podocytes using the Trizol reagent (Invitrogen, Milan, Italy). One or two μg of RNA underwent reverse transcription into cDNA using the High-Capacity Reverse Transcription kit (Applied Biosystems, Monza, Italy). TNFAIP2, podocin, nephrin, TGF-β1, LY6C2, MCP-1, CCR2 mRNA expression was quantitatively analysed by real time-PCR using the Applied Biosystems TaqMan reagents and pre-developed assays [*Tnfaip2* (Mm00447578_m1), *Nphs2* (Mm00499929_m1), *Nphs1* (Mm00497828_m1), *Tgfb1* (Mm00441724_m1), *Ly6c2* (Mm00841873_m1), *Ccl2* (Mm00441242_m1), *Ccr2* (Mm00438270_m1)]. Relative quantification was carried out using the $2^{-\Delta\Delta Ct}$ method. Results were normalized to the expression of appropriate housekeeping genes (HPRT, WT-1, 18S, GAPDH).

3.6 Protein analysis

Immunohistochemistry. Immunohistochemistry was performed in 4 µm-paraffin sections of formalin-fixed tissue. After antigen retrieval in a citrate buffer (0.01M, pH=6.0), sections were exposed to 3% H_2O_2 to neutralize endogenous peroxidase activity and endogenous avidin-binding sites were blocked by sequential incubation with 0.1% avidin and 0.01% biotin. Sections were then incubated with 3% bovine serum albumin (BSA) for blocking the aspecific binding sites. Sections were then incubated overnight at 4°C with primary antibodies directed against TNFAIP2 (Santa Cruz Biotechnology), rabbit anti-podocin (Sigma-Aldrich), rat anti-MAC-2 (Cederlane), and rabbit anti-p57 (Santa Cruz Biotechnology). After washing with PBS, sections were exposed to secondary biotinylated-labelled antibodies (swine anti-rabbit and rabbit anti-mouse from DAKO and goat anti-rat, from Jackson Immuno Research Laboratories) for 1 hour, followed by incubation with horseradish peroxidase (HRP)-conjugated streptavidin (DAKO) for 1 hour. 3,3'-diaminobenzidine (DAB) was used as a chromogen substrate for HRP. Sections were visualized with an Olympus-BX4I microscope and digitized with a high-resolution camera (Carl Zeiss, Germany). On average 30 randomly selected glomeruli from both outer and inner cortex were assessed per mouse. Results were expressed either as the number of positive cells/glomerular area or as percentage area of positive staining per glomerulus.

Immunofluorescence. Sections were fixed in cold acetone for 5 minutes and blocked in 3% BSA. Subsequently, sections were incubated overnight with primary antibodies: rabbit anti-podocin (Sigma Aldrich), guinea pig anti-nephrin (PROGEN, Germany), and rabbit anti-fibronectin (Sigma-Aldrich). Following washing with PBS, FITC-conjugated secondary antibodies (swine anti-rabbit, DAKO; goat anti-guinea pig, Santa Cruz Biotechnology) were incubated for 1 hour.

Results were expressed as percentage of positively stained tissue within the glomerular tuft. On average, 30 randomly selected glomeruli from both outer and inner cortex were assessed per mouse.

Double immunofluorescence. Paraffin sections of formalin-fixed tissue underwent antigen retrieval in citrate buffer. Sections were blocked with avidin-biotin solutions and 3% BSA and then incubated overnight at 4°C with a primary antibody made in rabbit and directed against TNFAIP2 (Santa Cruz Biotechnology). After washing with PBS, sections were subsequently incubated with a biotin-labelled secondary antibody (DAKO, swine anti-rabbit biotinylated) for 1 hour and AlexaFluor-488-conjugated avidin (Thermo Fisher Scientific, Italy) for 1 hour. After further blocking in 3% BSA, sections were incubated with a primary antibody against synaptopodin (mouse monoclonal, PROGEN, Germany) for 18 hours at 4°C, followed by incubation with an RPE-conjugated secondary antibody (DAKO, rabbit anti-mouse-RPE). Digitalized images were color-combined and assembled into photomontages by using Adobe Photoshop (Universal Imaging Corporation, West Chester, PA).

Protein extraction and immunoblotting. Podocytes were homogenized in a modified RIPA buffer containing 0.5% (vol/vol) NP40, 0.5% (wt/vol) sodium deoxycholate, 0.1% (wt/vol) sodium dodecyl sulphate (SDS), 10 mM EDTA, and protease inhibitors (aprotinin, leupeptin and PMSF, purchased from Sigma-Aldrich). After sonication and a 45-minute incubation in ice, protein extracts were obtained by centrifugation at 12,000xg for 20 minutes at 4°C. Total protein concentration was determined using the DC Protein Assay kit (Bio-Rad, Italy). Equal amounts of protein samples were separated by electrophoresis on a SDS polyacrylamide gel and electro-

transferred to a nitrocellulose membrane (all equipment and reagents used for immunoblotting were purchased from Bio-Rad, Italy). Following blocking in 5% non-fat milk/TBS (pH=7.6), membranes were incubated with a primary antibody made in rabbit and directed against TNFAIP2 (Santa Cruz Biotechnology) overnight at 4°C. After washing with TBS, membranes were probed with a secondary HRP-linked antibody (Amersham, donkey anti-rabbit-HRP) for 1 hour. Detection was performed using the chemiluminescent substrate Super Signal PICO (Euroclone, Italy) and visualized using a Bio-Rad Gel-Doc system. Band-signal intensities were quantified by densitometry. Tubulin was used as a loading control.

3.7 Statistical analysis.

Data were expressed as means ± SEM, geometric mean (25^{th}-75^{th} percentile), and fold change over control. Non-normally distributed variables were log-transformed prior to the analyses. Data were analyzed by the Student's t test or ANOVA, as appropriate. Least significant difference test was used for post-hoc comparisons. Values of $P<0.05$ were considered statistically significant.

4. Results

4.1 TNFAIP2 expression in human diabetic nephropathy

TNFAIP2 expression was studied in renal cortex sections obtained from patients with DN and non-diabetic control subjects (Table 2). TNFAIP2 was weakly expressed in normal renal cortex, but TNFAIP2 staining was significantly increased in patients with DN. Semi-quantitative analysis revealed a fourfold increase in the percentage positive area compared to controls. Of interest an increased TNFAIP2 expression was also observed in kidney biopsies from patients with microalbuminuria. This suggests that TNFAIP2 upregulation is an early event in the natural history of the complication (Figure 4A, B). In patients with DN, the pattern of staining suggested a predominant podocyte distribution and this was confirmed by colocalization of TNFAIP2 and synaptopodin staining in double immunofluorescence (Figure 4C).

Table 2. Clinical parameters of non-diabetic control subjects and patients with diabetic nephropathy (DN)

	Controls	**DM**
n	8	15
Age (years)	65.4 ± 6.3	66.5 ± 2.8
Sex (Male/Female)	6/2	11/4
Diabetes duration (years)	-	19.5 ± 0.7
Systolic bood pressure(mmHg)	120 ± 2.2	143 ± 4.6
Diastolic blood pressure (mmHg)	65 ± 3.1	83 ± 4.2
Serum creatinine (mg/dl)	1 ± 0.1	2.1 ± 0.4
Proteinuria (g/24 h)	-	2.1 ± 0.5
Hypertension (%)	-	100

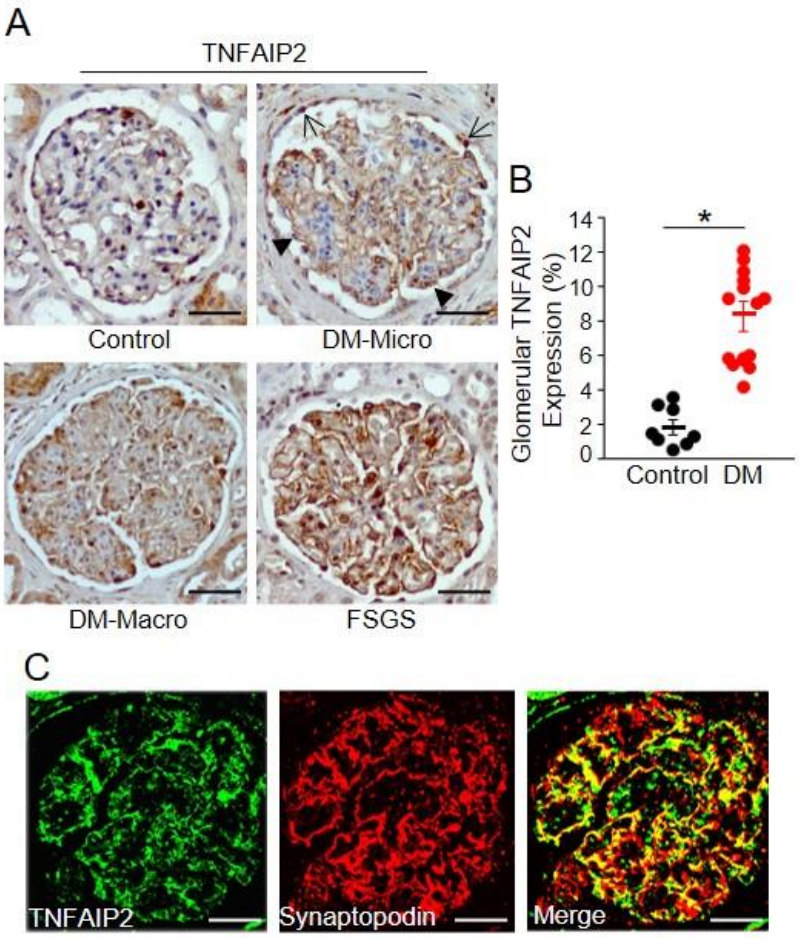

Figure 4. TNFAIP2 expression in human diabetic nephropathy. (A) Glomerular TNFAIP2 protein expression was assessed by immunohistochemistry in renal cortex sections from control subjects (*n*=8) and patients with either incipient (DM-micro, *n*=3) or overt diabetic nephropathy (DM-macro, *n*=12) [podocyte (arrowheads)] (original magnification 200X, scale bar=100 µm). Focal segmental glomerulosclerosis (FSGS) sections were used as a positive control. **(B)** The percent area of positive staining, quantified by a computer-aided image analysis system, is shown in the graph (*p<0.001 DM vs. controls). **(C)** Double immunofluorescence for TNFAIP2 and the podocyte marker synaptopodin was carried out on renal sections from DM patients. Merged images showed co-localization (original magnification 200X, scale bar=100 µm).

4.2 TNFAIP2 expression in experimental diabetes.

TNFAIP2 expression was assessed in an animal model of diabetes (STZ-induced diabetes). After 12 weeks of diabetes, TNFAIP2 protein expression was greater in diabetic (DM) compared to non-diabetic (ND) mice (Figure 5A, B). Podocytes were the predominant glomerular cell type overexpressing TNFAIP2, as confirmed by staining for both TNFAIP2 and podocin on serial renal cortex sections (Figure 5C). Consistent with this, TNFAIP2 mRNA levels were almost threefold higher in the glomeruli from diabetic animals (Figure 5D).

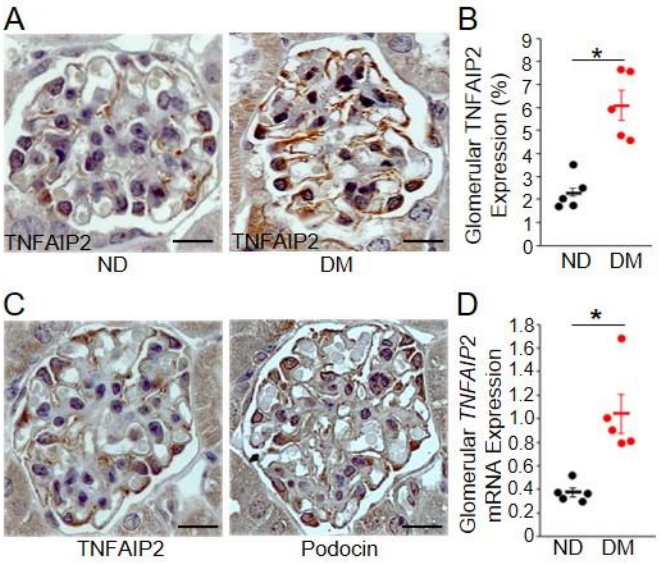

Figure 5. TNFAIP2 expression in experimental diabetic nephropathy. (A) Representative immunohistochemistry images of glomerular TNFAIP2 protein expression in renal cortex sections from non-diabetic (ND) and diabetic mice (DM) after 12 weeks of diabetes (magnification 400X, scale bar=50 µm). **(B)** Quantification of the percentage of glomerular TNFAIP2-positive staining is reported in the graph (*n*=5 mice per group; *p<0.001 DM vs. ND). **(C)** Staining for podocin and TNFAIP2 on serial renal cortical sections obtained from DM mice, showing a predominant podocyte distribution (magnification 400X, scale bar=50 µm). **(D)** TNFAIP2 mRNA levels were measured in glomeruli isolated from both ND and DM mice by real time-PCR and corrected for the expression of the housekeeping gene HPRT (*n*=5 mice per group; *p<0.001 ND vs. DM).

4.3 Generation of global TNFAIP2 KO mice (C57BL6 background)

TNFAIP2-knock out (KO) mice on a Balb/c background (FSGS prone strain) spontaneously develop FSGS. To clarify if this effect was strain-dependent, we generated TNFAIP2-KO mice on a C57BL6 genetic background (FSGS resistant strain) [75-77] (Figure 6).

Homozygotes TNFAIP2-KO C57BL6 mice were viable, born at normal Mendelian ratios, and grew normally. At variance with Balb/c mice, these animals had a normal renal phenotype, even after long-term follow-up, and at 26 weeks of age there was no difference in ACR between WT and TNFAIP2-KO mice (WT 25.76 ± 2.09 vs. KO 29.01 ± 1.32; mean ± ESM, p=NS).

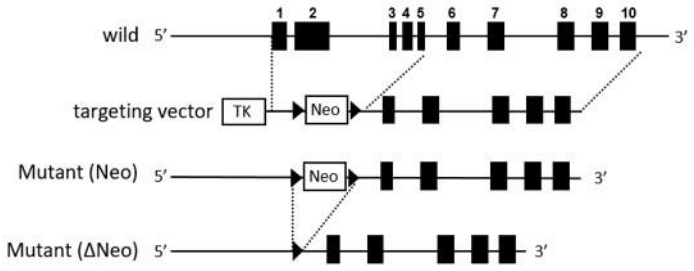

Figure 6. **Schematic illustration of the strategy for generating TNFAIP2-KO mice by deletion of gene exons 1 to 5.**

4.4 Effect of TNFAIP2 deletion on metabolic and physiological parameters.

Diabetes was induced in both WT and TNFAIP2-KO C57Bl6 mice by STZ administration. After 12 weeks of diabetes, blood glucose and glycated hemoglobin levels were similar in diabetic TNFAIP2-KO and WT mice. In addition, TNFAIP2 deletion did not alter body weight and kidney

weight-to-body weight (KW/BW) ratio. Finally, no difference was observed in systolic blood pressure (BP) among groups (Table 3).

4.5 Effect of TNFAIP2 deletion on albuminuria and renal function

There was a significant increase in ACR in DM compared to ND animals after 12 weeks of diabetes. TNFAIP2 deletion did not affect albuminuria in controls, but markedly increased albuminuria in DM animals. Furthermore, a significant reduction in creatinine clearance was specifically observed in diabetic TNFAIP2-KO mice compared to the other groups (Table 3).

Table 3. Metabolic and physiological parameters in wild type and TNFAIP2-KO mice

	ND-WT	ND-KO	DM-WT	DM-KO
Body Weight (g)	30.20 ± 0.97	28.92 ± 1.73	21.65 ± 1.31[a]	20.80 ± 0.86 [a]
Blood Glucose (mg/dl)	136.20 ± 2.80	150.70 ± 8.30	403.30 ± 40.1 [a]	382.50 ± 23.90 [a]
Glycated Hb (%)	4.75 ± 0.15	5.12 ± 0.10	10.92 ± 0.55 [a]	11.41 ± 0.33 [a]
Systolic BP (mmHg)	108.00 ± 3.20	105.00 ± 3.10	103.00 ± 1.30	106.00 ± 2.50
KW/BW ratio	6.61 ± 0.32	5.45 ± 0.21	7.57 ± 2.11[b]	7.45 ± 0.42[b]
ACR (µg/mg)	36.80 ± 7.70	28.80 ± 7.90	68.20 ± 14.00[b]	144.10 ± 36.50[c]
Cr Cl (ml/min)	0.43 ± 1.37	0.40 ± 3.20	0.31 ± 3.74	0.17 ± 0.050[d]

Data are expressed as mean ± ESM; ND: non-diabetic; DM: diabetic; KW/BW kidney weight/body weight; ACR albumin-to-creatinine ratio; Cr Cl creatinine clearance; [a]$p<0.001$; [b]$p<0.05$ DM groups vs. ND groups; [c]$p<0.05$ DM-KO vs. DM-WT; [d]$p<0.05$ DM-KO vs. others.

4.6 Podocyte abnormalities

To clarify the underlying mechanism of the detrimental effect of TNFAIP2 deletion, we assessed podocyte abnormalities. We found a significant downregulation of both podocin and nephrin in DM mice and this effect was exacerbated by TNFAIP2 deletion. On the contrary, lack of TNFAIP2 did not affect podocin/nephrin expression in ND mice (Figure 7A, B). Both podocin and nephrin mRNA levels were diminished in DM mice and this effect was even greater in DM TNFAIP2-KO animals (Figure 7C).

Diabetes-induced podocyte foot process effacement was enhanced in DM mice lacking TNFAIP2 (Figure 7D), as assessed by electron microscopy. The number of both podocytes and apoptotic podocytes was similar in DM and ND animals in this model of early DN; however, in diabetic mice, TNFAIP2 deletion reduced the number of differentiated podocytes, and enhanced the number of apoptotic podocytes (Figure 7E, F).

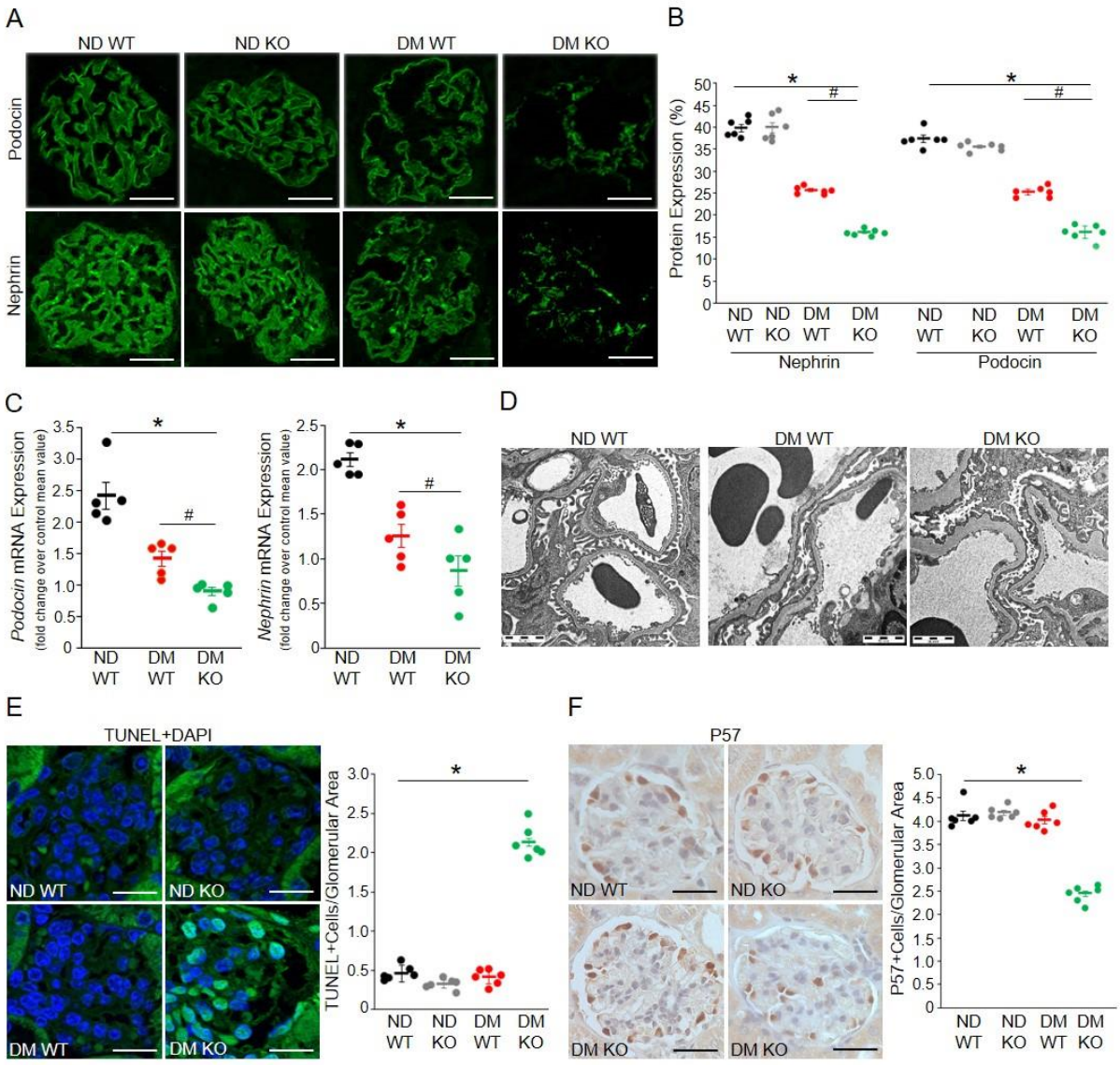

Figure 7. Effect of TNFAIP2 deficiency on diabetes-induced podocyte abnormalities Renal cortex samples from ND-WT, ND-KO, DM-WT, and DM-KO mice were studied 12 weeks after diabetes onset. Podocin and nephrin both protein and mRNA expression were assessed by immunofluorescence and real time-PCR, respectively. Representative immunofluorescence images of podocin and nephrin **(A)** are shown (magnification 400X, scale bar=50 µm) and **(B)** quantification of glomerular staining reported in the graph (*n*=5-6 mice per group; ∗p<0.001 DM groups vs. ND groups; #p<0.05 DM-KO vs. DM-WT). **(C)** Nephrin and podocin mRNA levels were measured by real-time PCR in total renal cortex and corrected for the expression of the WT-1 gene (n= 5 mice per group; ∗p<0.001 DM groups vs. ND #p<0.05 DM-KO vs. DM-WT). **(D)** Electron microscopy images showing glomeruli from ND-WT, DM-WT and DM-KO mice. The

extent of foot processes effacement was greater in DM-KO than in DM-WT animals (magnification 3200X). **(E)** Apoptosis was assessed by TUNEL assay (green) and nuclei counterstained with DAPI (magnification 400X, scale bar=50μm). The percentage of apoptotic cells is shown in the graph (n=6 mice per group; ∗p<0.001 DM-KO vs. others). **(F)** Representative immunohistochemistry images of p57 staining are shown (magnification 400X, scale bar=50 μm). The graph shows the number of podocytes (p57-positive cells) per glomerulus (n=6 per group; ∗p<0.001 DM-KO vs. others).

4.7 Mesangial expansion and glomerulosclerosis

Histological assessment by PAS staining revealed a mild mesangial expansion and scattered tubulointerstitial damage in DM mice. The degree of glomerular injury was greater in DM TNFAIP2-KO mice. Indeed, a more prominent mesangial expansion was observed by both light and electron microscopy (Figure 8A-C). Furthermore, diabetes-induced fibronectin protein expression was exacerbated in DM mice lacking TNFAIP2 (Figure 8D, E). Similarly, mRNA expression of the pro-sclerotic cytokines TGF-β1 was greater in DM TNFAIP2-KO compared to DM WT animals (Figure 8F).

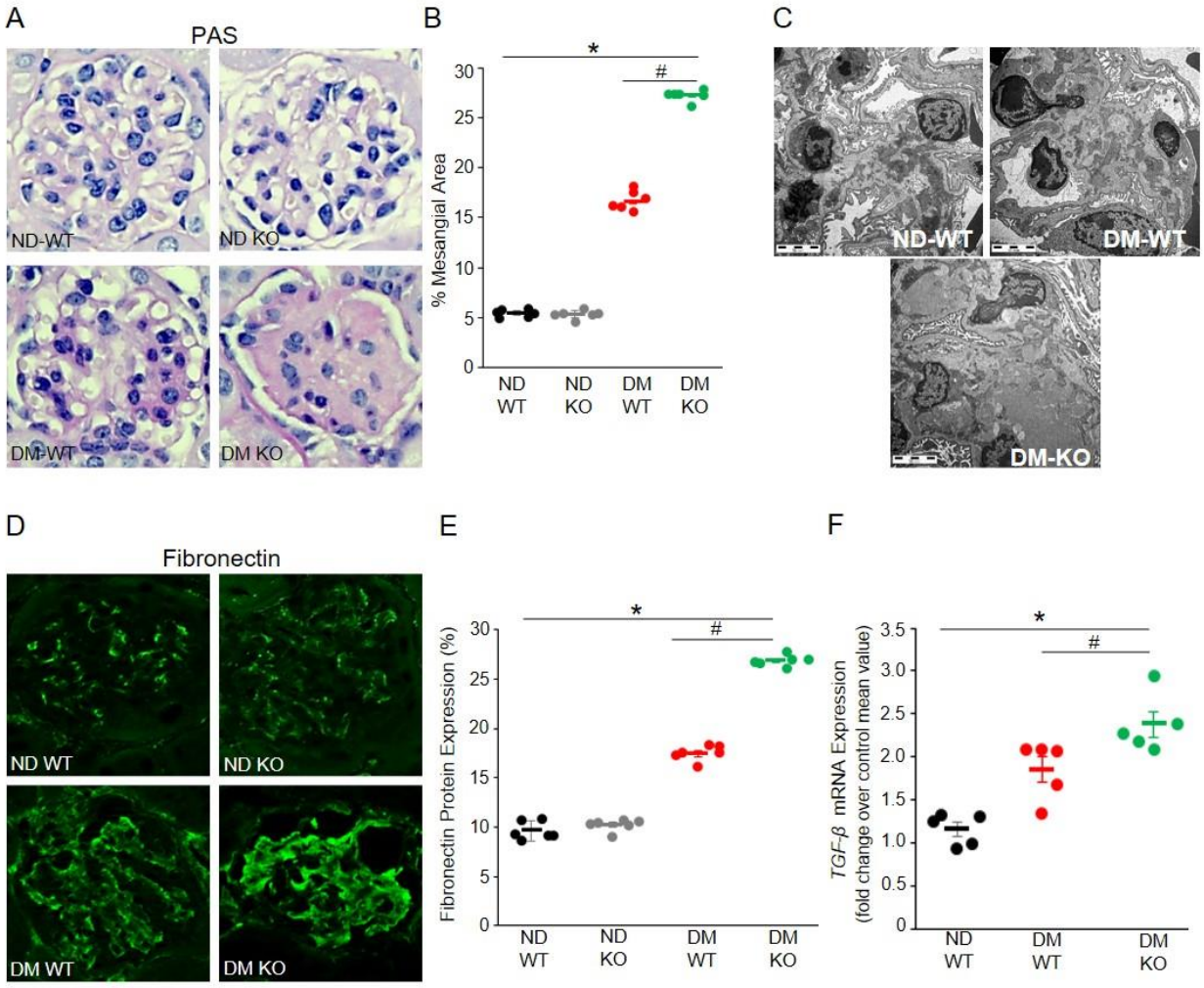

Figure 8. Effect of TNFAIP2 deletion on diabetes-induced glomerular structural abnormalities and expression of markers of fibrosis. Renal cortex samples from ND-WT, ND-KO, DM-WT, and DM-KO mice were studied 12 weeks after diabetes onset. **(A)** Representative PAS staining images (magnification 400X, scale bar=50µm) and **(B)** quantitation of glomerulosclerosis are shown (n=6 mice per group; ∗p<0.001 DM groups vs. ND groups; #p<0.05 DM-KO vs. DM-WT). **(C)** Electron microscopy images showing a more prominent mesangial expansion in the glomeruli from DM-KO mice compared to DM-WT mice. **(D)** Immunofluorescence images of glomerular fibronectin are shown (magnification 400X, scale bar=50µm) and **(E)** quantification of glomerular staining is reported in the graph (n=6 mice per group; ∗p<0.001 DM groups vs. ND groups; #p<0.05 DM-KO vs. DM-WT). **(F)** TGF-β1 mRNA levels were measured by real-time PCR in total renal cortex and corrected for the expression of the housekeeping gene HPRT (n=5; ∗p<0.001 DM groups vs. ND; #p<0.05 DM-KO vs. DM-WT).

4.8 Inflammation

The number of glomerular cells positive for the macrophage marker MAC-2 was greater in DM than ND animals. The absence of TNFAIP2 further increased diabetes-induced macrophage accrual without affecting glomerular macrophage infiltration in ND mice (Figure 9A). The expression of both LY6C2 and MCP-1 was significantly increased in DM mice and this effect was exacerbated by TNFAIP2 deletion (Figure 9B, C). Diabetes did not alter expression of the MCP-1 receptor CCR2; however, CCR2 overexpression was observed in diabetic TNFAIP2-KO mice (Figure 9D).

TNFAIP2 is highly expressed by monocytes/macrophages and inflammation plays a key role in DN; therefore, we performed a bone marrow (BM) transplantation study to assess the potential role of TNFAIP2 expressed in BM cells on the renal phenotypes of DM TNFAIP2-KO mice (Figure 9E). Transplantation of BM cells from WT mice to KO mice did not rescue the renal phenotype of diabetic TNFAIP2-KO mice as both albuminuria and glomerulosclerosis were similar in DM-KO-c^{KO} and DM-KO-c^{WT} (Table 4 and Figure 9F, G). This indicates that BM-derived cells did not play a major role in the enhanced glomerular injury observed in DM TNFAIP2-KO mice.

Table 4. Metabolic and physiological parameters in the BM transplantation study

	ND-WT-c^{WT}	**ND-KO-c^{KO}**	**DM-WT-c^{WT}**	**DM-KO-c^{KO}**	**DM-KO-c^{WT}**
BW (g)	26.02 ± 0.33	26.42 ± 0.51	22.19 ± 0.83[a]	21.77 ± 0.75[a]	22.85 ± 1.52[a]
BG (mg/dl)	124.2 ± 3.64	123.4 ± 3.07	381.0 ± 1.15[b]	397.0 ± 11.70[b]	384.0 ± 34.90[b]
Glycated Hb (%)	4.82 ± 0.19	5.06 ± 0.12	10.48 ± 0.25[b]	10.64 ± 0.26[b]	10.54 ± 0.31[b]
SBP (mmHg)	114.20 ± 5.27	111.20 ± 4.59	108.80 ± 1.15	112.60 ± 1.60	111.4 ± 1.77
KW/BW ratio	5.85 ± 0.01	5.99 ± 0.01	7.29 ± 0.56[c]	7.40 ± 0.10[c]	7.30 ± 0.64[c]

AER (µg/18h)	19.60 (18.80-19.10)	22.12 (20.20-22.30)	51.46[d] (34.90-66.00)	87.63[e] (77.60-107.90)	84.87[e] (64.30-117.20)

Data are expressed as mean ± ESM or geometric mean (25°-75° percentile); ND non-diabetic; DM diabetic; SBP Systolic Blood Pressure; BW body weight; BG blood glucose; KW/BW kidney weight/body weight; AER Albumin Excretion Rate; [a]p<0.05 [b]p<0.001; [c]p<0.01 DM groups vs. ND groups; [d]p<0.05 DM-WT-c^{WT} vs. ND groups; [e]p<0.05 DM-KO-c^{KO} and DM-KO-c^{WT} vs. DM-WT-c^{WT}.

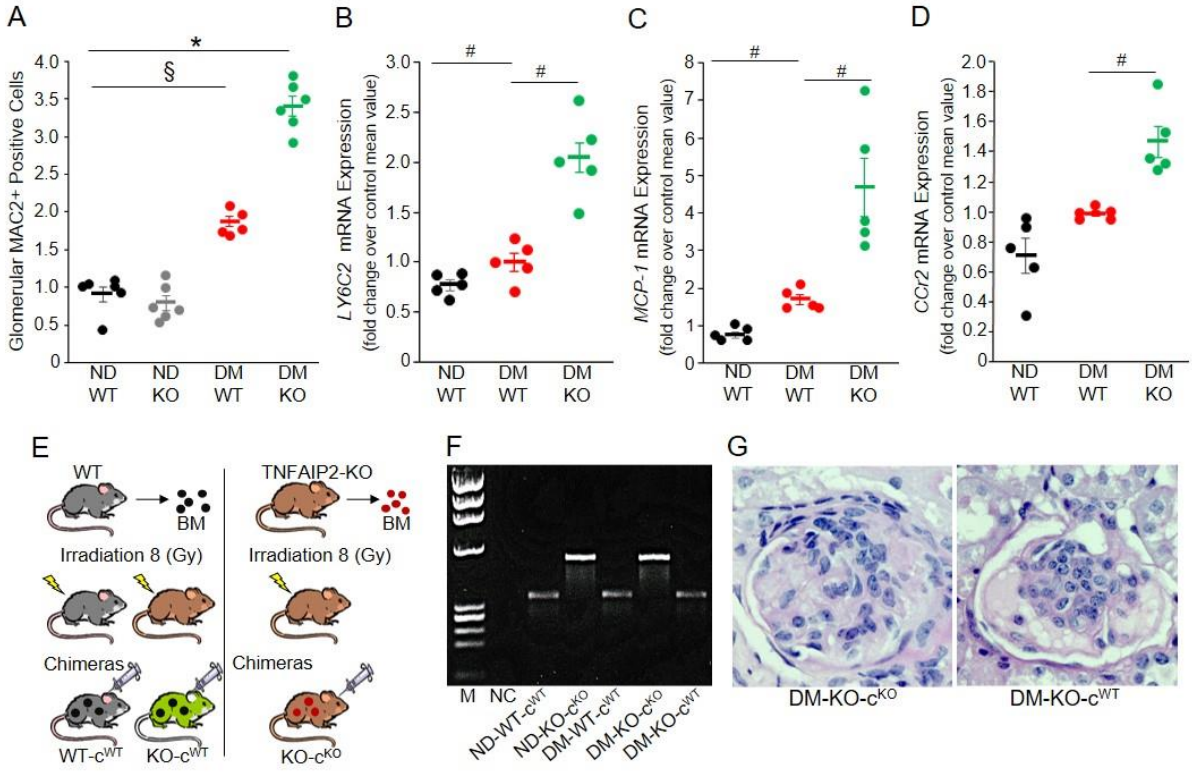

Figure 9. Markers of inflammation and chimeric animals. Renal cortex samples from ND-WT, ND-KO, DM-WT, and DM-KO mice were studied 12 weeks after diabetes onset. **(A)** Glomerular macrophage accrual was evaluated by counting the number of MAC-2 positive cells per glomerulus (n=6 mice per group; §p<0.001 DM-WT vs. ND groups; *p<0.001 DM-KO vs. others). **(B-D)** LY6C2, MCP-1, and CCR2 mRNA levels were measured in the renal cortex obtained from ND-WT, DM-WT, and DM-KO animals by real time-PCR and corrected for the expression of the housekeeping gene HPRT (n=5 mice per group; *p<0.001; §p<0.001; #p<0.05 DM-WT vs. ND-WT; #p<0.05 DM-KO vs. DM-WT). **(E)** Schematic illustration of the protocol used for generating

chimeric mice. Recipient WT and TNFAIP2-KO mice were sub-lethally irradiated, and then reconstituted with BM from either WT (WT-c^{WT}; KO-c^{WT}) or TNFAIP2-KO (KO-c^{KO}) mice. **(F)** PCR genotyping of peripheral blood cells from chimeric animals. M: marker; NTC: no template control **(G)** Representative images of PAS staining of renal cortex sections from DM TNFAIP2-KO mice transplanted with BM cells from either KO or WT animals. (magnification 200X, scale bar=100μm).

4.9 Effect of diabetes-related insults on TNFAIP2-TNT system in cultured podocytes

We have previously reported that podocytes exposed to serum deprivation and Adriamycin form TNTs via a TNFAIP2-dependent mechanism [71]. Herein, we assessed if diabetes-related insults also induce the TNFAIP2-TNT system in cultured podocytes.

An over two-fold increase in TNFAIP2 both protein and mRNA expression were observed in high glucose (HG)-treated podocytes as compared to control cells (Figure 10A, B, C). By contrast, no changes in TNFAIP2 mRNA levels were observed in podocytes exposed to either glycated-albumin (GA) or mechanical stretch (Figure 10D, E).

Podocyte formed TNT-like structures (Figure 11A) that fulfill the morphological criteria of TNTs, including the presence of an actin backbone (Figure 11B) and the lack of contact to the substrate (Figure 11C, D). Exposure to both GA and HG resulted in a greater number of podocytes connected by TNTs as compared to controls and this effect was abolished by TNFAIP2 silencing (Figure 11E, F, G). Additionally, treatment with either the Akt inhibitor VIII (1 μM), or the PI3K inhibitor LY-294002 (50 μM) prevented the high glucose-induced TNT formation (Figure 11H).

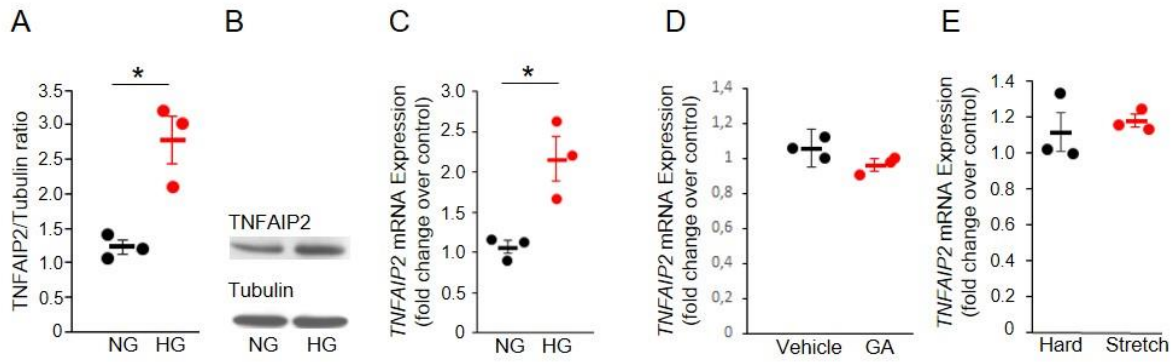

Figure 10. TNFAIP2 expression in cultured podocytes exposed to diabetes-related insults. (A, B) TNFAIP2 protein expression was assessed in podocytes exposed to HG (30mM) or normal glucose concentrations (NG = 10mM) for 48h. Representative immunoblotting image (tubulin was used a loading control) and results of densitometry analysis are shown (*n*=3; *p<0.001 HG vs. NG). TNFAIP2 mRNA levels were measured by real-time PCR in podocytes exposed to (**C**) NG/HG for 48h (*n*=3; *p<0.001 HG vs. NG), **(D)** glycated-albumin (GA, 1.2 µg/ml) for 48h (*n*=4, p=ns), and **(E)** mechanical stretch (10% elongation) for 24h (*n*=3, p=ns). 18s/GAPDH were used as housekeeping genes.

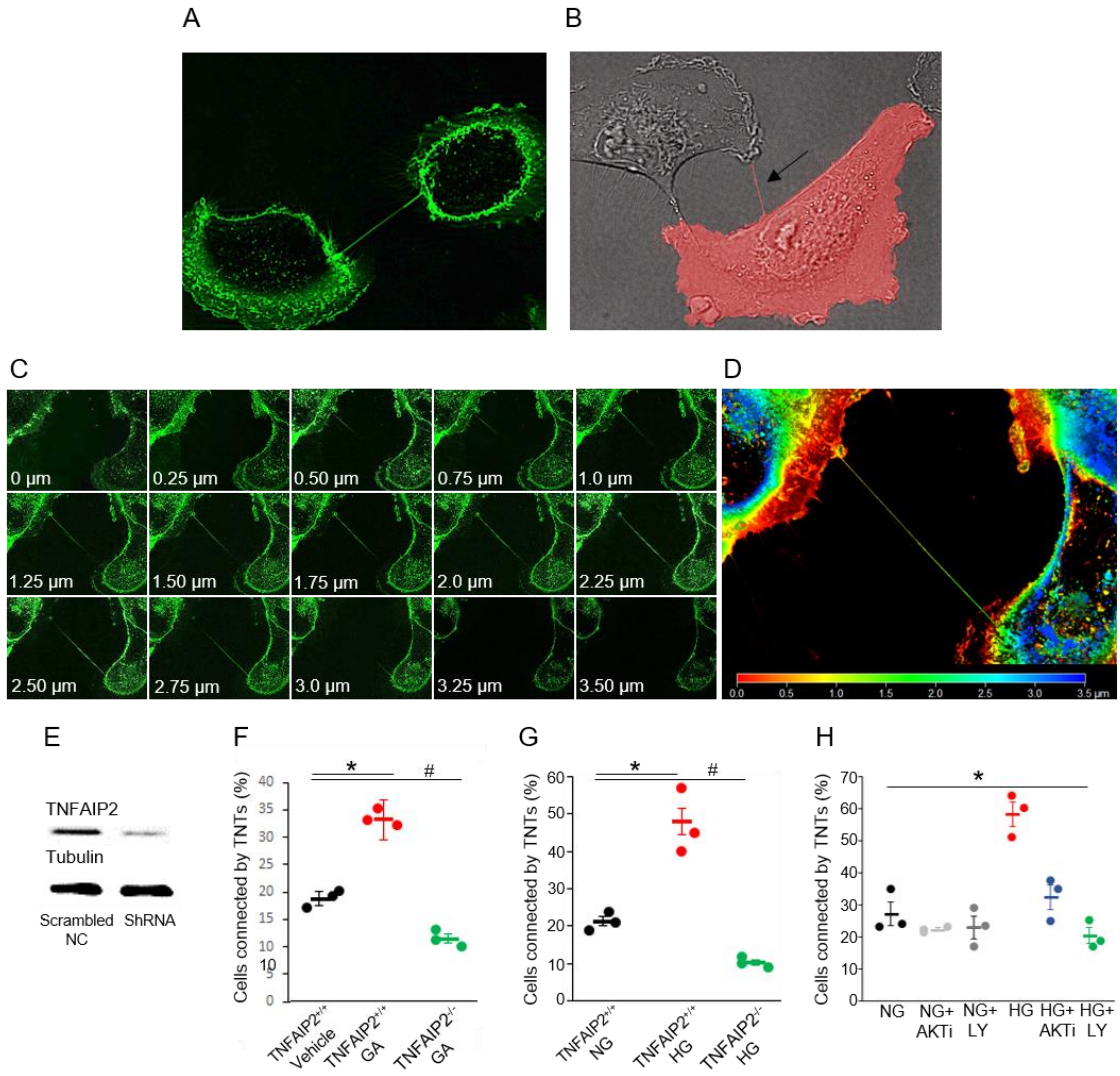

Figure 11. TNFAIP2-dependent TNT formation in cultured podocytes exposed to diabetes-related insults.

(A) Podocytes pre-exposed to high glucose (HG) were stained with WGA Alexa Fluor-488 to reveal TNTs. A representative image showing a TNT-like channel, interconnecting two podocytes, is shown (magnification 630X, scale bar=50µm). **(B)** The image shows that TNTs bridging podocytes contain actin. Actin was labeled with Cell-Light Actin-RFP (magnification 630X, scale bar=50µm). **(C)** Serial Z-stack images, acquired with a step-size of 0.25 µm proved that TNTs did not adhere to the substrate. In panel **D**, colors represent the Z-depth (depth coding; red: bottom, blue: top). **(E)** Podocytes were transfected with either TNFAIP2 shRNA ($TNFAIP2^{-/-}$) or a mock plasmid ($TNFAIP2^{+/+}$) and knockdown efficiency assessed by immunoblotting (tubulin was used

a loading control). **(F-G)** Cells were exposed to either GA or HG for 48h, stained with WGA Alexa-488, and analyzed by fluorescent live cell microscopy to reveal TNTs (magnification 630X, scale bar=50µm). As shown in graphs F and G, the percentage of podocytes connected by one or more TNTs was enhanced by both GA and HG and almost abolished by TNFAIP2 silencing [(*HG experiments*. *n*=3; *p<0.001 TNFAIP2$^{+/+}$HG vs. TNFAIP2$^{+/+}$NG; #p<0.01 TNFAIP2$^{-/-}$HG vs. TNFAIP2$^{+/+}$NG); (*GA experiments*. *n*=3; *p<0.001 TNFAIP2$^{+/+}$GA vs. TNFAIP2$^{+/+}$Vehicle; #p<0.01 TNFAIP2$^{-/-}$GA vs. TNFAIP2$^{+/+}$Vehicle)]. **(H)** Podocytes were exposed either to NG or HG in the presence or absence of either the AKT VIII inhibitor (1µM) or the PI3K inhibitor LY-294002 (50 µM) for 48h, stained with WGA Alexa-488, and analyzed by fluorescent live cell microscopy. The graph shows the percentage of podocytes connected by one or more TNTs (*n*=3; *p<0.001 HG vs. others).

4.10 TNT-mediated transfer of mitochondria between cultured podocytes

To test if TNTs interconnecting podocytes *in vitro* were functionally active, we focused on mitochondria. To induce podocyte damage, Cell-Tracker-Blue-labeled podocytes (recipient cells) were exposed to GA and then co-cultured with donor podocytes labeled with mitochondria (Red MitoTracker).

Red fluorescent mitochondria were found along TNTs and in the cytosol of recipient blue cells, indicating mitochondrial transfer (Figure 12A). By contrast, no transfer was observed when TNT formation was prevented by physical separation of donor and recipient cells sharing the same culture medium (Figure 12B).

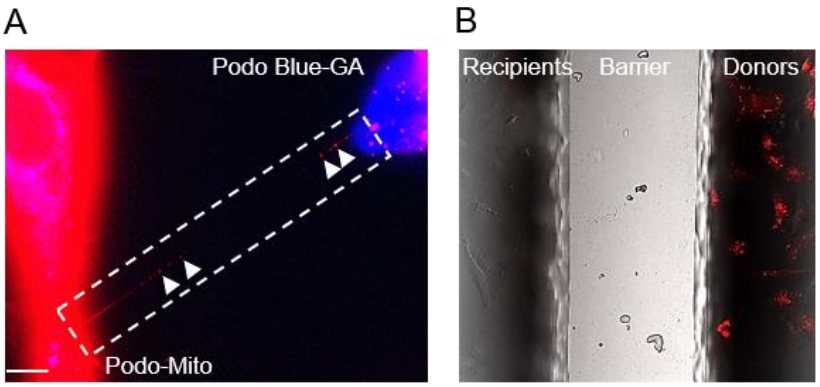

Figure 12. TNTs allow mitochondrial transfer between podocytes. (A) Podocytes stained with Cell-Tracker Blue were pre-exposed to glycated albumin (GA, 1.2 µg/ml) for 48 hours and then co-cultured with donor podocytes labeled with MitoTracker. The image shows RFP-mitochondria within the TNT and in the cytosol of a blue-stained recipient podocyte (magnification 630X, scale bar = 50 µm). **(B)** GA-treated podocytes and normal donor podocytes containing MitoTracker-labeled mitochondria were separately seeded in a two-well Ibidi culture insert. After removal of the insert, the two populations were co-cultured for 24 hours. As shown in the representative image, RFP-labeled mitochondria were not observed in recipient cells.

5. Summary of results

Human study	**Cortical kidney biopsies analysis:** To assess TNFAIP2 glomerular expression in human DN	↑ TNFAIP2 expression in DN patients (including microalbuminuric) ↑ TNFAIP2 expression particularly in podocytes (colocalization with synaptopodin)
Animal studies	**STZ-induced diabetes mouse model (C57Bl/6):** To assess TNFAIP2 glomerular expression in experimental DN	↑ TNFAIP2 expression and mRNA levels in DM mice (12 weeks after DM onset) ↑ TNFAIP2 expression particularly in podocytes (colocalization with podocin)
	TNFAIP2 global KO mouse model (C57Bl/6): To study the effects of TNFAIP2 genetic deletion on the functional, structural, and molecular alterations of DN	**PHYSIOLOGICAL AND METABOLIC PARAMETERS** (Results: DM-KO compared to DM-WT): - ↑ ACR - ↓ CrCl **RENAL TISSUE ANALYSES** (Results: DM-KO compared to DM-WT): - *PODOCYTE ABNORMALITIES* (↓ expression of slit diaphragm proteins, ↑ foot process effacement, ↓ podocyte number, and ↑ podocyte apoptosis) - ↑ GLOMERULOSCLEROSIS (↑ mesangial expansion, ↑ expression of fibronectin, ↑ mRNA levels of TGF-β1) - ↑ INFLAMMATION (↑ glomerular macrophage accrual; ↑ mRNA levels of Ly6c2; MCP-1/CCR2)

	Chimeric mice: To evaluate the contribution of BM-derived cells on the renal phenotype of DM-KO mice	TNFAIP2 deletion from BM cells does not contribute to the functional and structural alterations observed in DM-KO mice (AER and PAS staining: DM-KO-c^{KO} = DM-KO-c^{WT})
***In vitro* studies**	**Cultured podocytes:** 1. To test if DM-related insults induce the TNFAIP2-TNT system	- ↑ TNFAIP2 expression after exposure to HG - ↑ number of podocytes connected via TNTs after exposure to either HG or GA - HG/GA-induced TNT formation is TNFAIP2-dependent - HG-induced TNT formation is mediated by PI3K and AKT
	2. To test if TNTs interconnecting podocytes *in vitro* are functionally active	- TNTs mediate transfer of mitochondria from donor podocytes to recipient podocytes pre-exposed to GA

6. Discussion

This study provides evidence that TNFAIP2 is overexpressed by podocytes in both human and experimental DN. Of interest, glomerular TNFAIP2 overexpression was also observed in patients with microalbuminuria, though the number of patients was very small. This suggests that TNFAIP2 induction may be an early event in the natural history of human DN. Consistent with this hypothesis, an increase in glomerular TNFAIP2 was also found in an early phase of experimental diabetes.

Our *in vitro* data showing that exposure of podocytes to high glucose concentrations increased TNFAIP2 expression provides a potential mechanism whereby diabetes enhances podocyte TNFAIP2 expression. TNFAIP2 is also overexpressed by podocytes in patients with FSGS [71]. This raises the possibility that TNFAIP2 induction is a common response to podocyte injury in various chronic glomerulopathies.

We have previously reported that TNFAIP2 deletion induces the spontaneous development of FSGS in Balb/c mice. However, TNFAIP2-KO mice on a C57BL6 background did not show any renal abnormality. This suggests that development of a renal phenotype in TNFAIP2-KO mice is strain-dependent. Differences in the susceptibility to develop FSGS between the Balb/c and the C57BL6 strain have been previously reported [73, 78]. For instance, Adriamycin induces FSGS in Balb/c mice, while C57BL6 are resistant to FSGS development [79]. On the other hand, in diabetic C57BL6 mice lack of TNFAIP2 worsened both albuminuria and renal function, implying that diabetes-induced glomerular injury is required to disclose the renal protective effect of TNFAIP2 in the C57BL6 mouse strain.

Diabetic mice lacking TNFAIP2 had an increase in nephrin/podocin downregulation, foot process effacement, and podocyte apoptosis/loss, providing a potential mechanism for the worsening in diabetes-induced albuminuria. In this early model of experimental diabetes, renal function was still normal in diabetic WT mice. However, a significant renal function loss was observed in diabetic TNFAIP2-KO animals. Enhanced expression of fibrosis markers and glomerulosclerosis in diabetic TNFAIP2-KO mice likely contributed to early renal function decline.

Importantly, body weight, blood glucose levels, glycated hemoglobin, and systolic blood pressure were similar in WT and TNFAIP2 KO diabetic mice, indicating that the effects observed were independent of both metabolic and hemodynamic factors.

Inflammatory processes have also been implicated in the pathogenesis of DN [35]. Deletion of TNFAIP2 exacerbated diabetes-induced glomerular inflammation as shown by both increased glomerular monocyte accrual and MCP-1/CCR2 overexpression. However, transplantation of BM cells from TNFAIP2-KO mice in WT animals and vice versa did not modify the phenotype of recipient diabetic animals. This together with the observation that TNFAIP2 overexpression occurred predominantly in podocytes in both human and experimental DN suggests that TNFAIP2 deletion in podocytes rather than in immune/inflammatory cells played a major role in exacerbating DN.

Worsening of DN in TNFAIP2 KO mice suggest that TNFAIP2 has a protective role in the kidney and that podocyte TNFAIP2 overexpression in DN is a mechanism to counteract podocyte injury. Our *in vitro* experiments aimed to investigate the underlying mechanisms of the protective effect of TNFAIP2 suggest that TNFAIP2-dependent TNT formation may be involved. TNTs are membrane channels bridging distant cells and allowing intercellular exchange of various cargos [43, 46, 49}. We found that exposure of podocytes to either high glucose or glycated-albumin

(GA) enhanced the formation of intercellular membrane bridges that fulfilled the morphological criteria for the definition of TNTs. Specifically, these membranous structures were straight, exhibited a width of less than 0.5 μm and a length of several cell diameters, and contained a F-actin/tubulin backbone [43]. These structures did not adhere to the substrate, as assessed by Z-stack reconstruction, and this is a specific feature of TNTs that differentiate them from filopodia [44]. TNTs have been described in various cell types *in vitro*, including podocytes [71]; however, herein we provide the first evidence that diabetes-related insults can induce TNT formation. TNTs form *de novo* predominantly from stressed cells and our results demonstrates that the cellular stress induced by podocyte exposure to high glucose and GA is sufficient to trigger TNT formation.

Importantly, diabetes-induced TNT-formation in podocytes was almost abolished in TNFAIP2$^{-/-}$ podocytes, indicating a TNFAIP2-dependent effect. Consistent with this, previous studies have shown that TNFAIP2 cooperates with the RalA small GTPase and the exocyst complex to trigger F-actin polymerization and TNT formation [67, 70]. However, dependency on TNFAIP2 for TNT formation is cell-type specific and we have previously shown that TNT formation in tubular epithelial cell is independent of TNFAIP2 [71]. Diabetes-induced TNT formation was also prevented by Akt and PI3K inhibition, suggesting an important role of these intracellular signaling molecules in regulating TNT formation in podocytes.

At variance with other cell-to-cell communication system, TNTs allows the exchange of cellular organelles, including mitochondria and lysosomes [43, 49, 50, 61]. This is of relevance in the context of diabetes because organelle dysfunction plays an important role in the pathogenesis of DN. To provide evidence that diabetes-induced TNTs were functionally active and could allow replacement of dysfunctional organelles, we focused on mitochondria as TNFAIP2 deletion induces mitochondrial alterations in Balb/c mice and horizontal TNT-mediated mitochondrial

transfer occurs in Adriamycin-treated podocytes. Our *in vitro* results confirmed that exposure of podocytes to GA induced mitochondrial transfer between podocytes *via* TNTs. Although mitochondria are quite large, recent studies using correlative cryoelectron microscopy confirmed that mitochondrial transfer through TNTs is feasible as mitochondria can enlarge TNTs, creating a bulge [80].

TNT-mediated horizontal mitochondrial transfer in diabetic podocytes is of potential functional relevance as mitochondrial abnormalities, such as swollen/fragmented mitochondria, altered mitochondrial membrane potential, and impaired permeability transition, have been demonstrated in renal cells exposed to a diabetic milieu and in the kidneys from diabetic animals. Moreover, the unifying hypothesis postulates that excessive generation of mitochondrial superoxide by hyperglycemia is the primary initiating event that activates all other pathways of glomerular damage in diabetes. Finally, hyperglycemia-induced mitochondrial oxidative stress can cause mtDNA mutations that can accumulate in terminally differentiated cells, such as podocytes, leading to alterations in mitochondrial bioenergetics [24-29].

Whether TNT-mediated mitochondrial transfer can rescue recipient podocytes remains to be established. However, studies in other cell types showed that transferred mitochondria ameliorate mitochondrial performance of recipient cells and even restore aerobic respiration in cells lacking mitochondria [50, 52-55]. Moreover, we have previously demonstrated in podocytes that TNT-mediated mitochondrial transfer ameliorates injury of podocytes exposed to Adriamycin/serum deprivation [71]. On the other hand, intercellular exchange of mitochondria *via* TNTs may be less effective as a protective mechanism in pathological conditions, such as diabetes, in which all cells are exposed to an identical dangerous milieu.

Although the deleterious effect of TNFAIP2 deletion in DN is likely mediated by prevention of TNT-mediated exchange, other TNT-independent mechanisms cannot be excluded. Indeed, TNFAIP2 interacts with small GTPases, regulating actin dynamics that are crucial for podocyte function in DN [67] Moreover, TNFAIP2 is also a downstream target of retinoic acid and TNFAIP2 deficiency may be involved in retinoic acid-induced podocyte differentiation [39].

In conclusion, diabetes induces TNFAIP2 expression in podocytes. In experimental DN, lack of TNFAIP2 magnifies podocyte damage, glomerulosclerosis, and renal dysfunction. This suggests that podocyte TNFAIP2 overexpression in diabetes is a compensatory mechanism aimed to limit diabetes-induced glomerular injury. *In vitro* experiments have provided a possible explanation for the beneficial effects of TNFAIP2. Indeed, exposure to diabetes-related insults induced TNT formation between podocytes via a TNFAIP2-dependent mechanism. Moreover, TNTs bridging podocytes were functionally active as they allowed the transfer of mitochondria.

References

1. IDF Diabetes Atlas 9th Edition 2019. https://www.diabetesatlas.org/en/
2. Afkarian M, Zelnick LR, Hall YN, Heagerty PJ, Tuttle K, Weiss NS, de Boer IH. *Clinical Manifestations of Kidney Disease Among US Adults With Diabetes*, 1988-2014. JAMA 2016; 316:602-10.
3. Levin A, Tonelli M, Bonventre J, Coresh J, Donner J-A, Fogo AB, Fox CS, Gansevoort RT, Heerspink HJL, Jardine M, Kasiske B, Köttgen A, Kretzler M, Levey AS, Luyckx VA, Mehta R, Moe O, Obrador G, Pannu N, Parikh CR, Perkovic V, Pollock C, Stenvinkel P, Tuttle KR, Wheeler DC, Eckardt K-U, ISN Global Kidney Health Summit participants. *Global kidney health 2017 and beyond: a roadmap for closing gaps in care, research, and policy*. Lancet 2017; 390:1888-1917.
4. Saran R, Robinson B, Abbott KC, et al. *US Renal Data System 2018 Annual Data Report: Epidemiology of Kidney Disease in the United States*. Am J Kidney Dis 2019; 79:A7-A8.
5. The Diabetes Control and Complications (DCCT) Research Group. *Effect of intensive therapy on the development and progression of diabetic nephropathy in the Diabetes Control and Complications Trial*. Kidney Int 1995; 47:1703-20.
6. UK Prospective Diabetes Study (UKPDS) Group. *Intensive blood-glucose control with sulphonylureas or insulin compared with conventional treatment and risk of complications in patients with type 2 diabetes (UKPDS 33).* Lancet 1998; 352:837-53.
7. Diabetes Control and Complications Trial/Epidemiology of Diabetes Interventions and Complications Research Group: Lachin JM, Genuth S, Cleary P, Davis MD, Nathan DM. *Retinopathy and nephropathy in patients with type 1 diabetes four years after a trial of intensive therapy*. N Engl J Med 2000; 342:381-9.
8. Retnakaran R, Cull CA, Thorne KI, Adler AI, Holman RR; UKPDS Study Group. *Risk factors for renal dysfunction in type2 diabetes: U.K. Prospective Diabetes Study 74*. Diabetes 2006; 55: 1832–1839.
9. Bakris GL,Weir MR, Shanifar S, Zhang Z, Douglas J, van Dijk DJ, Brenner BM; RENAAL Study Group. *Effects of blood pressure level on progression of diabetic nephropathy: Results from the RENAAL study*. Arch Intern Med 2003; 163: 1555–1565.
10. Pohl MA, Blumenthal S, Cordonnier DJ, De Alvaro F, Deferrari G, Eisner G, Esmatjes E, Gilbert RE, Hunsicker LG, de Faria JB, Mangili R, Moore J r., Reisin E, Ritz E, Schernthaner G, Spitalewitz S, Tindall H, Rodby RA, Lewis EJ. *Independent and additive impact of blood pressure control and angiotensin II receptor blockade on renal outcomes in the irbesartan diabetic nephropathy trial: Clinical implications and limitations*. J Am Soc Nephrol 2005; 16: 3027–3037.
11. Tuttle KR, Bakris GL, Bilous RW, Chiang JL, de Boer IH, Goldstein-Fuchs J, Hirsch IB, Kalantar-Zadeh K, Narva AS, Navaneethan SD, Neumiller JJ, Patel UD, Ratner RE, Whaley-Connell AT, Molitch ME. *Diabetic kidney disease: a report from an ADA Consensus Conference.* Diabetes Care 2014; 37:2864-2883.

12. Papa C, Giunti S, Gruden G (2021). Diabete mellito e ipoglicemie – Nefropatia Diabetica, in Rugarli C (8th Edition). *Medicina Interna Sistematica*. Trento: edra, pp.1671-1673.
13. Alicic RZ, Rooney MT and Tuttle KR. *Diabetic Kidney Disease. Challenges, Progress and Possibilities.* Clin J Am Soc Nephrol. 2017; 12:2032-2045
14. Nagata M. *Podocyte injury and its consequences*. Kidney Int. 2016; 86:1221-1230.
15. Doublier S, Ruotsalainen V, Salvidio G, Lupia E, Biancone L, Conaldi PG, Reponen P, Tryggvason K, Camussi G. *Nephrin redistribution on podocytes is a potential mechanism for proteinuria in patients with primary acquired nephrotic syndrome.* Am J Pathol 2001; 158:1723-1731.
16. Benigni A, Gagliardini E, Tomasoni S, Abbate M, Ruggenenti P, Kalluri R, Remuzzi G. *Selective impairment of gene expression and assembly of nephrin in human diabetic nephropathy*. Kidney Int 2004; 65:2193-2200.
17. Mason RM, Wahab NA. *Extracellular matrix metabolism in diabetic nephropathy*. J Am Soc Nephrol 2003; 14:1358-73.
18. Gruden G, Cavallo Perin P, Camussi G. *Insight on the pathogenesis of diabetic nephropathy from the study of podocyte and mesangial cell biology*. Curr Diabetes Rev 2005; 1:27-40.
19. Susztak K, Raff AC, Schiffer M, Erwin P Böttinger EP. *Glucose-induced reactive oxygen species cause apoptosis of podocytes and podocyte depletion at the onset of diabetic nephropathy.* Diabetes 2006; 55:255-33.
20. Schena FP, Gesualdo L. *Pathogenetic mechanisms of diabetic nephropathy*. J Am Soc Nephrol 2005; 1:S30-3.
21. Sun YM, Su Y, Li J, Wang L-F. *Recent advances in understanding the biochemical and molecular mechanism of diabetic nephropathy*. Biochem Biophys Res Commun 2013; 433-359-61.
22. Ding Y, Choi ME. *Autophagy in Diabetic Nephropathy*. J Endocrinol 2015; 224:R15-R30.
23. Hartleben B, Gödel M, Meyer-Schwesinger C, Liu S, Ulrich T, Köbler S, Wiech T, Grahammer F, Arnold SJ, Lindenmeyer MT, et al. *Autophagy influences glomerular disease susceptibility and maintains podocyte homeostasis in aging mice*. Journal of Clinical Investigation 2010; 120:1084–1096.
24. Coughlan MT, Thorburn DR, Penfold SA, Laskowski A, Harcourt BE, Sourris KC, et al. *RAGE-induced cytosolic ROS promote mitochondrial superoxide generation in diabetes*. J Am Soc Nephrol 2009; 20:742-752.
25. Oliveira PJ, Esteves TC, Seiça R, Moreno AJ, Santos MS. *Calcium-dependent mitochondrial permeability transition is augmented in the kidney of Goto-Kakizaki diabetic rat*. Diabetes Metab Res Rev. 2004; 20:131-136.
26. Wang W, Wang Y, Long J, Wang J, Haudek SB, Overbeek P, et al. *Mitochondrial fission triggered by hyperglycemia is mediated by ROCK1 activation in podocytes and endothelial cells*. Cell Metab 2012; 15:186-200.
27. Qiu W, Zhou Y, Jiang L, Fang L, Chen L, Su W, et al. *Genipin inhibits mitochondrial uncoupling protein 2 expression and ameliorates podocyte injury in diabetic mice*. PLoS One. 2012; 7:e41391.

28. Nishikawa T, Edelstein D, Du XL, Yamagishi S, Matsumura T, Kaneda Y, et al. *Normalizing mitochondrial superoxide production blocks three pathways of hyperglycaemic damage*. Nature. 2000; 404:787-790.
29. Forbes JM, Thornburn DR. *Mitochondrial dysfunction in diabetic kidney disease*. Nat Rev Nephrol 2018; 14:291-312.
30. Ruggenenti P, Cravedi P, Remuzzi G. *The RAAS in the pathogenesis and treatment of diabetic nephropathy*. Nat Rev Nephrol 2010; 6:319-330.
31. Riser BL, Cortes P, Heilig C, Grondin J, Ladson-Wofford S, Patterson D, Narins RG. *Cyclic stretching force selectively up-regulates transforming growth factor-beta isoforms in cultured rat mesangial cells*. Am J Pathol 1996; 148:1915–1923.
32. Gruden G, Zonca S, Hayward A, Thomas S, Maestrini S, Gnudi L, Viberti GC. *Mechanical stretch-induced fibronectin and transforming growth factor-beta1 production in human mesangial cells is p38 mitogen-activate protein kinase-dependent*. Diabetes 2000; 49:655–661.
33. Endlich N, Kress KR, Reiser J, Uttenweiler D, Kriz W, Mundel P, Endlich K. *Podocytes respond to mechanical stress in vitro.* J Am Soc Nephrol 2001; 12:413– 422.
34. Petermann AT, Hiromura K, Blonski M, Pippin J, Monkawa T, Durvasula R, Couser WG, Shankland SJ. *Mechanical stress reduces podocyte proliferation in vitro*. Kidney Int 2002; 61:40 –50.
35. Barutta F, Bruno G, Grimaldi S, Gruden G. *Inflammation in diabetic nephropathy: moving towards clinical biomarkers and targets for treatment*. Endocrine 2015; 48:730-742.
36. C. Sassy-Prigent, D. Heudes, C. Mandet, M.F. Belair, O. Michel, B. Perdereau, J. Bariety, P. Bruneval, *Early glomerular macrophage recruitment in streptozotocin-induced diabetic rats*. Diabetes 2000; 49:466–475.
37. F.Y. Chow, D.J. Nikolic-Paterson, E. Ozols, R.C. Atkins, B.J. Rollin, G.H. Tesch, *Monocyte chemoattractant protein-1 promotes the development of diabetic renal injury in streptozotocin-treated mice*. Kidney Int 2006; 69:73–80.
38. Omote K, Gohda T, Murakoshi M, Sasaki Y, Kazuno S, Fujimura T, Ishizaka M, Sonoda Y, Tomino Y. *Role of the TNF pathway in the progression of diabetic nephropathy in KK-Ay mice.* Am. J Physiol Renal Physiol 2014; 306: F1335-F1347.
39. Saito Y, Okamura M, Nakajima S, Hayakawa K, Huang T, Yao J, Kitamura M. *Suppression of nephrin expression by TNF-alpha via interfering with the cAMP-retinoic acid receptor pathway.* Am J Physiol Renal Physiol 2010; 298: F1436-1444.
40. Chow FY, Nikolic-Paterson DJ, Ma FY, Ozols E, Rollins BJ, Tesch GH. *Monocyte chemoattractant protein 1-induced tissue inflammation is critical for the development of renal injury but not type 2 diabetes in obese db/db mice*. Diabetologia 2007; 50:471–480.
41. Tarabra E, Giunti S, Barutta F, Salvidio G, Burt D, Deferrari G, Gambino R, Vergola D, Pinach S, Cavallo Perin P, Camussi G, Gruden G, *Effect of the monocyte chemoattractant protein-1/CC chemokine receptor 2 system on nephrin expression in streptozotocin-treated mice and human cultured podocytes*. Diabetes 2009; 58:2109–2118.
42. Barutta F, Bernardi S, Gargiulo G, Durazzo M, Gruden G. *SGLT2 inhibition to address the unmet needs in diabetic nephropathy*. Diabetes Metab Res Rev 2019; 35:e3171.

43. Rustom A, Saffrich R, Markovic I, Walther P, Gerdes HH. *Nanotubular highways for intercellular organelle transport*. Science 2004; 303:1007–1010.
44. Delage E, Cordero Cervantes D, Penard E, Schmitt C, Syan S, Disanza A, Scita G, Zurzolo C. *Differential identity of Filopodia and Tunneling Nanotubes revealed by the opposite functions of actin regulatory complexes*. Sci Rep 2016; 6:39632.
45. Takahashi A, Kukita A, Li Y, Zhang J, Nomiyama H, Yamaza T, Ayukawa Y, Koyano K, Kukita T. *Tunneling nanotube formation is essential for the regulation of osteoclastogenesis*. J Cell Biochem 2013; 114:1238-47.
46. Wang X, Bukoreshtliev V, Gerdes HH. *Developing Neurons Form Transient Nanotubes Facilitating Electrical Coupling and Calcium Signaling with Distant Astrocytes*. PLoS One 2012; 7:e47429.
47. Sun X, Wang Y, Zhang J, Tu J, Wang XJ, Su XD, Wang L, Zhang Y. *Tunneling-nanotube direction determination in neurons and astrocytes*. Cell Death Dis 2012; 3:e438.
48. Zaccard CR, Watkins SC, Kalinski P, Fecek RJ, Yates AL, Salter RD, Ayyavoo V, Rinaldo CR, Mailliard RB. *CD40L induces functional tunneling nanotube networks exclusively in dendritic cells programmed by mediators of type 1 immunity*. J Immunol 2015; 194:1047-56.
49. Abounit S, Bousset L, Loria F, Zhu S, de Chaumont F, Pieri L, Olivo-Marin JC, Melki R, Zurzolo C. *Tunneling nanotubes spread fibrillar α-synuclein by intercellular trafficking of lysosomes.* EMBO J 2016; 35:2120-2138.
50. Spees JL, Olson SD, Whitney MJ, Prockop DJ. *Mitochondria transfer between cells can rescue aerobic respiration*. Proc Natl Acad Sci U S A 2006; 103:1283-8.
51. Pasquier J, Guerrouahen BS, Thawadi HA, Ghiabi P, Maleki M, Abu-Kaoud N, Jacob A, Mirshahi M, Galas L, Rafii S, Le Foll F, Rafii A. *Preferential transfer of mitochondria from endothelial to cance cells through tunneling nanotubes modulates chemoresistance*. J Transl Med 2013; 11:94.
52. Islam MN, Das SR, Emin MT, Wei M, Sun L, Westphalen K, Rowlands DJ, Quadri SK, Bhattacharya S, Bhattacharya J. *Mitochondrial transfer from bone-marrow-derived stromal cells to pulmonary alveoli protects against acute lung injury*. Nat Med 2012; 18:759-65.
53. Hayakawa K, Esposito E, Wang X, Terasaki Y, Liu Y, Xing C, Ji X, Lo EH. *Transfer of mitochondria from astrocytes to neurons after stroke.* Nature 2016; 535:551-5.
54. Cho YM, Kim JH, Kim M, Park SJ, Koh SH, Ahn HS, Kang GH, Lee JB, Park KS, Lee HK. *Mesenchymal stem cells transfer mitochondria to the cells with virtually no mitochondrial function but not with pathogenic mtDNA mutations*. PLoS One 2012; 7:e32778.
55. Wang X, Gerdes HH. *Transfer of mitochondria via tunneling nanotubes rescues apoptotic PC12 cells.* Cell Death Differ 2015; 22:1181-91.
56. Jansens RJJ, Tishchenko A, Favoreel HW. *Bridging the Gap: Virus Long-Distance Spread via Tunneling Nanotubes*. J Virol 2020; 94:e02120.
57. Gousset K, Zurzolo C. *Tunnelling nanotubes: a highway for prion spreading?* Prion 2009; 3:94-8.
58. Onfelt B, Nedvetzki S, Benninger RKP, Purbhoo MA, Sowinski S, Hume AN, Seabra MC, Neil MAA, French PMW, Davis DM. *Structurally distinct membrane nanotubes between human macrophages support long-distance vesicular traffic or surfing of bacteria*. J Immunol 2006; 177:8476-83.
59. Pinto G, Brou C, Zurzolo C. *Tunneling Nanotubes: The Fuel of Tumor Progression?* Trends Cancer 2020; 6:874-888.

60. Costanzo M, Abounit S, Marzo L, Danckaert A, Chamoun Z, Roux P, Zurzolo C. *Transfer of polyglutamine aggregates in neuronal cells occurs in tunneling nanotubes.* J Cell Sci 2013; 126:3678-85.
61. Victoria GS and Zurzolo C. *The spread of prion-like proteins by lysosomes and tunneling nanotubes: Implications for neurodegenerative diseases*. J Cell Biol 2017; 216:2633-2644.
62. Parker I, Evans KT, Ellefsen K, Lawson DA, Smith IF. *Lattice light sheet imaging of membrane nanotubes between human breast cancer cells in culture and in brain metastases.* Sci Rep 2017; 7:11029.
63. Weil S, Osswald M, Solecki G, Grosch J, Jung E, Lemke D, Ratliff M, Hänggi D, Wick W, Winkler F. *Tumor microtubes convey resistance to surgical lesions and chemotherapy in gliomas.* Neuro Oncol 2017; 19:1316-1326.
64. Alarcon-Martinez L, Villafranca-Baughman D, Quintero H, Kacerovsky JB, Dotigny F, Murai KK, Prat A, Drapeau P, Di Polo A. *Interpericyte tunnelling nanotubes regulate neurovascular coupling*. Nature 2020; 585:91-95
65. Sarma V, Wolf FW, Marks RM, Shows TB, Dixit VM. *Cloning of a novel tumor necrosis factor-alpha-inducible primary response gene that is differentially expressed in development and capillary tube-like formation in vitro*. J Immunol 1992; 148:3302-12.
66. Wolf FW, Sarma V, Seldin M, Drake S, Suchard SJ, Shao H, O'Shea KS, Dixit VM. *B94, a primary response gene inducible by tumor necrosis factor-alpha, is expressed in developing hematopoietic tissues and sperm acrosome*. J Biol Chem 1994; 269:3633-40.
67. Hase K, Kimura S, Takatsu H, Ohmae M, Kawano S, Kitamura H, Ito M, Watarai H, Hazalett CC, Yeaman C, Ohno H. *M-Sec promotes membrane nanotube formation by interacting with Ral and the exocyst complex*. Nat Cell Biol 2009; 11:1427-32.
68. Kimura S, Yamashita M, Yamakami-Kimura M, Sato Y, Yamagata A, Kobashigawa Y, Inagaki F, Amada T, Hase K, Iwanaga T, Ohno H, Fukaj S. *Distinct Roles for the N- and C-terminal Regions of M-Sec in Plasma Membrane Deformation during Tunneling Nanotube Formation*. Sci Rep 2016; 6:33548.
69. Wang Y, Cui J, Sun X, Zhang Y. *Tunneling-nanotube development in astrocytes depends on p53 activation*. Cell Death Differ 2011; 18: 732-42.
70. Schiller C, Diakopoulos KN, Rohwedder I, Kremmer E, von Toerne C, Ueffing M, Weidle UH, Ohno H, Weiss EH. *LST1 promotes the assembly of a molecular machinery responsible for tunneling nanotube formation*. J Cell Sci 2013; 126:767-77.
71. Barutta B, Kimura S, Hase K, Bellini S, Corbetta B, Corbelli A, Fiordaliso F, Barreca A, Papotti MG, Ghiggeri GM, Salvidio G, Roccatello D, Audrito V, Deaglio S, Gambino R, Bruno S, Camussi G, Martini M, Hirsch E, Durazzo M, Ohno H, Gruden G. *Protective Role of the M-Sec-Tunneling Nanotube System in Podocytes*. J Am Soc Nephrol 2021; ASN.2020071076
72. Lee VWS, Harris DCH. *Adriamycin nephropathy: a model of focal segmental glomerulosclerosis*. Nephrology 2011; 16:30-8.
73. Papeta N, Zheng Z, Schon EA, Brosel S, Altintas MM, Nasr SH, Reiser J, D'Agati VD, Gharavi AG. *Prkdc participates in mitochondrial genome maintenance and prevents Adriamycin-induced nephropathy in mice*. J Clin Invest 2010; 120:4055-64.
74. Dunn SR, Qi Z, Bottinger EP, Breyer MD, Sharma K. *Utility of endogenous creatinine clearance as a measure of renal function in mice*. Kidney Int 2004; 65:1959-67.
75. Ma LJ, Fogo AB. *Model of robust induction of glomerulosclerosis in mice: importance of genetic background*. Kidney Int 2003; 64:350-5.

76. Hartner A, Cordasic N, Klanke B, Veelken R, Hilgers KF. *Strain differences in the development of hypertension and glomerular lesions induced by deoxycorticosterone acetate salt in mice*. Nephrol Dial Transplant 2003; 18:1999-2004
77. Ishola DA, van der Giezen DM, Hahnel B, Goldschmeding R, Kriz W, Koomans HA, Joles JA. *In mice, proteinuria and renal inflammatory responses to albumin overload are strain-dependent*. Nephrol Dial Transplant 2006; 21:591-7.
78. Zheng Z, Schmidt-Ott KM, Chua S, Foster KA, Frankel RZ, Pavlidis P, Barasch J, D'Agati VD, Gharavi AG. *A mendelian locus on chromosome 16 determines susceptibility to doxorubicin nephropathy in the mouse*. Proc Natl Acad Sci U S A 2005; 102:2502-7.
79. Jeansson M, Björck K, Tenstad O, Haraldsson B. *Adriamycin alters glomerular endothelium to induce proteinuria*. J Am Soc Nephrol 2009; 20:114-22.
80. Sartori-Rupp A, Cordero Cervantes D, Pepe A, Gousset K, Delage E, Corroyer-Dulmont S, Schmitt C, Krijnse-Locker J, Zurzolo C. *Correlative cryo-electron microscopy reveals the structure of TNTs in neuronal cells*. Nat Commun 2019; 10:342.